Ediacaran-style Decay Experiments using Mollusks and Sea Anemones

By

Brandt Michael Gibson

Thesis

Submitted to the Faculty of the

Graduate School of Vanderbilt University

in partial fulfillment of the requirements

for the degree of

MASTER OF SCIENCE

in

Earth & Environmental Sciences

August 11, 2017

Nashville, Tennessee

Approved:

Simon A.F. Darroch, Ph.D.

Neil P. Kelley, Ph.D.

Ralf Bennartz, Ph.D.

ACKNOWLEDGMENTS

This project was made possible through two grants awarded to me: the Geological Society of America's Graduate Student Research Grant, and the Paleontological Society Student Grant — Harry B. Whittington Award. I would like to thank Drs. Marc Laflamme (University of Toronto Mississauga) and Neil Kelley (Vanderbilt University) for their invaluable discussions at various stages of this project, as well as Dr. Jim Schiffbauer and the University of Missouri X-ray Microanalysis Core Facility (MizzoμX) for the geochemical data acquisition. I would also like to thank my thesis committee (Drs. Ralf Bennartz, Neil Kelley, and Simon Darroch). More than any other influence associated with this project, I owe a great deal of gratitude and am indebted to my mentor and the chair of my committee, Dr. Simon Darroch, for the extensive guidance and support, as well as the freedom to make this project my own. Lastly, I would like to thank my family for their personal support throughout the past two years as I completed this project.

TABLE OF CONTENTS

LIST OF TABLES

Table Page

LIST OF FIGURES

CHAPTER 1

INTRODUCTION

The terminal Neoproterozoic Ediacara biota (575–541 Ma) is an enigmatic assemblage of large, morphologically complex eukaryotes that represents the first major radiation of multicellular life, and which may provide critical information surrounding early life evolutionary innovations in complex life forms (Erwin et al., 2011). Ediacaran organisms were entirely soft bodied, and possessed a variety of unusual morphologies that have no counterparts among extant animals. Most recent work suggests that they likely represent a polyphyletic grouping of several different eukaryotic lineages (Narbonne, 2005; Xiao and Laflamme, 2009; Darroch et al., 2015), although their unique body plans have led to them being collectively interpreted as occupying a variety of positions of the tree of life, including cnidarians (i.e., diploblasts; Hoffman, 1990; Conway Morris, 1993b), stem- and crown-group eumetazoans (mostly triploblasts, see e.g., Sokolov and Fedonkin, 1984), protists (Zhuravlev, 1993; Seilacher et al., 2003), lichens (Retallack, 1994), fungi (Peterson et al., 2003), and an entirely separate Kingdom of eukaryotic life – the 'Vendobionta' (Seilacher, 1989; Buss and Seilacher, 1994).

Despite 'uncertainly' in Ediacaran phylogenetic affinities, big strides have been made in understanding the mode in which these organisms were preserved. Fossils are typically found as casts and molds, which are attributed to the formation of pyritic 'death masks' (Gehling, 1999). In this model, Ediacaran organisms lived in close association with thick, sediment-surface microbial mats, which were widespread in Neoproterozoic shallow-marine settings (Seilacher and Pflueger, 1994; Seilacher, 1999; Noffke et al., 2002; Noffke, 2013). After death and rapid burial (for example, during a storm event), aerobic decay depleted oxygen in the sediment surrounding the organism and isolated dysoxic-anoxic pore waters surrounding the carcass from oxygenated water above the sediment-water interface. Sulfate reducing bacteria (SRBs) were then able to convert

sulfate (SO_2) to hydrogen sulfide (H_2S), which in turn combined with Fe in pore water to form a pyritic (FeS_2) 'death mask' that molded the external surface of the organism (Gehling, 1999; Gehling et al., 2005; Droser et al., 2006).

Strong empirical evidence in support of this model has been discovered in a majority of Ediacaran fossil localities, and from a wide variety of facies settings. For example, in shallow marine sandstones from South Australia, iron oxides and oxyhydroxides (i.e., the weathering products of pyrite) are commonly found between bedding planes preserving fossils (Wade, 1968; Schiffbauer et al., 2014; Tarhan et al., 2015; Liu et al., 2016). Pyritized microbial filaments have been discovered in association with Ediacaran fossil deposits in Russia (Callow and Brasier, 2009), and remineralized pyrite framboids have been described from deep water fossil surfaces associated with turbidite flows (Liu et al., 2015). In addition to empirical evidence from fossil surfaces, Darroch et al. (2012) were able to demonstrate incipient 'death mask' formation in decay experiments performed in the laboratory. Their study demonstrated a spatial association between Fe and S formed when organisms were decayed on microbial mats (although not in sufficient quantities to form the 'cement' around the outside of the organism envisaged in models), as well as the precipitation of aluminosilicate elements (specifically K, Al, Fe, and Mg) in association with a dark-colored 'halo' that expanded and contracted around carcasses over the course of decay. This evidence for clay mineral formation also provided a close match with clay layers that have long been found associated with Ediacaran fossils, and from a wide range of localities worldwide (Wade, 1968; Steiner and Reitner, 2001; Mapstone and McIlroy, 2006; Laflamme et al., 2010; Meyer et al., 2012, 2014; Tarhan et al., 2014). On this basis, Darroch et al. (2012) suggested that authigenic clay layers, rather than pyrite, may be the most important control on molding soft-tissue morphology and eventual fossil formation in Ediacaran taphonomic scenarios.

The Darroch et al. (2012) study therefore provided preliminary support for some key aspects of the 'death mask' model, but also raised several additional questions, in particular the relative importance of iron sulfides vs. clay minerals in molding the external surface of the

decaying carcasses. In addition, their experiments had significant shortcomings, including the choice of *Galleria mellonella* (a crown-group triploblast and ecdysozoan arthropod possessing a chitinous cuticle) as a decay organism, the use of freshwater (rather than marine) microbial mats, and the fact that they did not quantify the extent of FeS formation. Furthermore, the Darroch et al. (2012) experiments tested key tenets of the 'death mask' model, but did not design them in a way that allowed reinterpretation of actual Ediacaran fossils. Here, we expand upon the Darroch et al. study in order to address the following questions: (1) do Ediacaran-style taphonomic scenarios affect the 'normal' (i.e., open marine) pattern and rate of decay? (2) Do equivalent FeS 'death masks' form with both triploblastic and diploblastic organisms? (3) Are the dark decay 'halos' that formed in the Darroch et al. (2012) experiments consistently associated with the precipitation of aluminosilicate elements? (4) What is the rate and pattern of aluminosilicate precipitation as decay progresses? And finally: (5) what is the relative importance of FeS vs. clay minerals in molding the external morphology of carcasses, and thus in fossil preservation?

The answers to these questions allow a variety of potential interpretations surrounding the nature of Ediacaran organisms and paleoenvironments. For example, if patterns of character loss are not altered when organisms are decayed in Ediacaran-style taphonomic scenarios, then experiments using different organisms may potentially be used to interpret Ediacaran fossils (see Briggs, 2003; Sansom et al., 2010, 2011; Casenove et al., 2011; Nanglu et al., 2015; Briggs and McMahon, 2016; McMahon et al., 2017). Similarly, if FeS death masks form exclusively (or preferentially) with either diploblastic or triploblastic organisms, then this may allow us to constrain Ediacaran phylogenetic affinities. Lastly, contrasting the rates, patterns, and extent of FeS and aluminosilicate precipitation around carcasses will establish whether pyrite (Gehling, 1999; Schiffbauer et al., 2014; Cui et al., 2016) or clay minerals (e.g., Butterfield, 1995; Orr et al., 1998; Anderson et al., 2011; Darroch et al., 2012;) are potentially more important in Ediacaran fossilization. Alternatively, if neither FeS or clays form in sufficient quantities to justify a 'death

mask'-type model, then this could lend support to alternative explanations for Ediacaran soft-body preservation, such as that proposed by Tarhan et al. (2017) involving early silicification.

CHAPTER 2

METHODS

To address the questions listed above, we conducted two sets of experiments. The first experiment was used to create a baseline for rate and pattern of decay. We then repeated our decay experiments under Ediacaran-style conditions in order to: (1) compare differences in the rates and patterns of character loss; and, (2) to compare the degree of incipient pyritic or aluminosilicate 'death mask' formation. To compare rates and patterns of FeS and aluminosilicate precipitation within any decay 'halos' that formed, we analyzed sediment from around the carcasses using scanning electron microscopy energy dispersive x-ray analyses (SEM EDS).

2.1 Decay Organisms

As decay organisms, we used the giant sea anemone *Condylactis gigantea* (a diploblast), and the wedge sea hare *Dolabella auricularia* (a triploblast). We chose these organisms because of their relative large size, ready availability, and relative structural simplicity. Both organisms possess relatively few broad-scale morphological features that are unique to their species, and so can reasonably be claimed to typify the anatomy of their broader taxonomic groupings (actinians and opisthobranch gastropods, respectively). In addition, both these organisms belong to metazoan phyla that are thought to be have been present among the Ediacara biota. Several authors have noted similarities between Ediacaran frondose organisms and sea anemones (Gehling, 1991; Conway Morris, 1993a, 2000); *Inaria karli* (Gehling, 1988) in particular is interpreted as a cnidarian of actinian grade. The presence of actinians in the latest Precambrian is supported by molecular divergence dates, which suggest a split between Anthozoa and Medusozoa in the Ediacaran (Erwin et al., 2011; Park et al., 2012). The justification for using *D. auricularia* as a

decay organism is more complicated; no individual Ediacaran taxon has ever been interpreted as an opisthobranch mollusk specifically (although fossil examples are known from as early as the Carboniferous - Pek et al., 1996). However, the bilaterian taxon *Kimberella quadrata* (Glaessner and Wade, 1966) is interpreted as a stem-group mollusk (Fedonkin and Waggoner, 1997; Vinther, 2015; though not interpreted as so in Budd and Jensen, 2000), possessing a muscular foot, lineations interpreted as dorsoventral musculature, and a structurally rigid (but non-biomineralized) carapace (Fedonkin and Waggoner, 1997). Because opithobranchs possess many of these characteristics, we consider *D. auricularia* as a reasonable analogue for *Kimberella*, and a plausible model organism for possible Ediacaran triploblasts. However, there are obvious associated caveats; *Dolabella* is larger than the vast majority of *Kimberella* specimens, and secretes a more heavily biomineralized posterior carapace, both of which are attributes which may influence patterns of decay.

Condylactis gigantea anatomy.— Adult giant sea anemones, like most anemones, exist as polyps and are diploblastic organisms with radial symmetry. Figure 1 depicts the anatomy described here. They have an ectoderm and an endoderm, where the endoderm is differentiated into mesenteries, retractor muscles, pharynx, mesoglea, gametic tissue, and the gastrodermis. Like virtually all actinians, *Condylactis* has a radial oral disc surrounded by tentacles. This opening descends into a folding of the epidermis, known as the pharynx. The pharynx opens into the gastrovascular cavity, which is divided by multiple mesenteries. These mesenteries progress from the body wall toward the pharynx, with only some mesenteries connecting all the way to the pharynx.

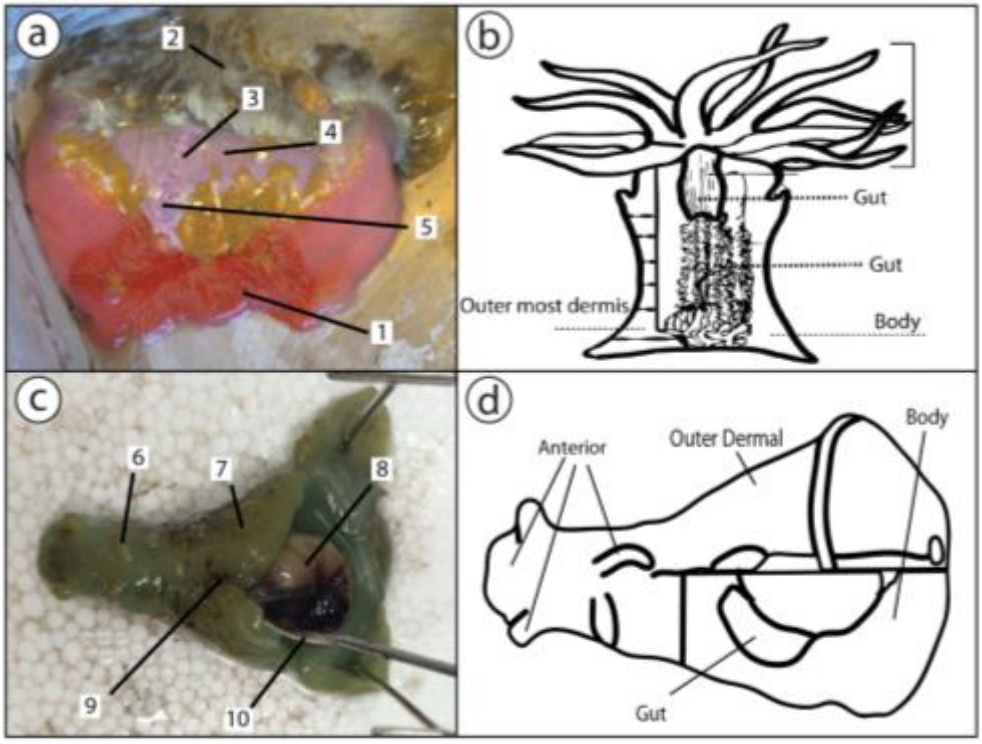

Figure 1. Comparative Anatomy of Decay Organisms: (a) Image of *Condylactis gigantea*, the giant sea anemone, outlining anatomy. (b) Generalized anatomical characters of *C. gigantea* used for decay indices. (c) Annotated image of *Dolabella auricularia*, the wedge sea hare. (d) Generalized anatomical characters of *D. auricularia* used for decay indices. Labelled portions for (a) include (1) pedal "foot", (2) tentacles, (3) pharynx, (4) mesenteries, (5) gametic tissue, and (b) include (6) rhinopore, (7) outer dermis, (8) gland, (9) siphonal incurrent, (10) posterior calcareous plate.

Dolabella auricularia anatomy.— Sea hares, mollusks similar to nudibranchs, are triploblastic organisms that have bilateral symmetry (Fig. 1). The external morphology of these organisms includes two rhinopores for sensing on the anterior end, a seminal groove between the anterior and posterior regions, and connecting incurrent and excurrent siphons on the posterior end. The anterior region is approximately one-third as narrow as the posterior region, which includes a calcareous shell that protects internal glands and gill from the incurrent via the siphonal flap. Musculature is arranged in a similar fashion to most marine opisthobranches, in which there are longitudinal somatic muscles running the length of the organism used for swimming.

Comparative anatomy and construction of decay indices.— We chose anatomical features to score for decay stages that were architecturally broad; this was done in order to facilitate

easier comparisons with Ediacaran fossils (which in many localities tend not to preserve fine-scale anatomical details), and easier comparisons between decay organisms. These included the anterior region, outer dermal layer, 'gut' tissue, and dorsoventral body tissue. These encompassed multiple smaller scale features that were described during the decay process, but that were ultimately lumped into their respective groups (hereafter referred to as 'characters'). Anterior region characters included the tentacle region on *Condylactis*, and the head region of *Dolabella* containing the rhinopores. 'Gut' tissue in our anemones represents the gametogenic tissues as well as the pharynx. The same label was applied to the sea hare internal glands, gill, and various related organs. Body tissue character for the organisms included the mesenteries and muscles of the anemones and the locomotion muscles of the sea hares. Characters for both organisms are shown in Figure 1.

Decay indices were generated by assigning a numerical decay state (DS) value to the characters described above, with each value representing proportional amount of anatomical loss. Values were scaled from 1 – 4 (DS1, DS2, etc.), with values of 1 representing 0-25% loss of a specified feature, DS2, 25-50% loss, etc. Features that received a value of 4 indicated that 75-100% of that feature had been lost to decay. Observed features were generalized for easy comparison between diploblastic and triploblastic organisms (e.g. outer dermal layer, "gut", "body tissue", and "anterior region").

2.2 Decay Experiments

Baseline decay experiments.— We purchased decay organisms from an online aquarium retailer (see Supplemental Material ESM1). We euthanized organisms by placing them in a mixture of magnesium chloride hexahydrate ($MgCl_2*6H_2O$) at 50:50 ratio (Cameron, 2002; Nanglu et al., 2015); this method has the advantage of not introducing foreign chemicals (which may affect either tissue lability or the composition of decay biota - American Veterinary Medical Association, 2013),

but instead merely overdoses the organisms with the same chemical species they would naturally encounter in marine settings (Brusca, 1980). Organisms were then rinsed with artificial seawater (AWS; specific gravity =1.02), weighed, photographed, and placed in decay vessels. For decay vessels, we used 120 mL screw lid jars with 2 mm mesh lining the bottom (modified from Nanglu et al., 2015). The mesh placement allowed for us to more easily remove carcasses and organic matter that were positioned at the bottom of decay vessels. Once specimens were deposited in vessels, ~60 mL of AWS were added to each vessel. Vessels were then sealed with lids and placed in a Heracell VIOS i160 tri-gas incubator which allowed us to control environmental conditions. Even though the vessels were sealed, for these experiments, we approximated extant atmospheric compositions 79% N, 0.1% CO_2, 21% O_2, and maintained a constant temperature of 25°C.

We sampled decaying organisms and observed the state/pattern of decay after 1, 2, 3, 4, 6, 8, 12, 17, 18, and 38 days. We chose these sampling intervals based on the rate of decay of each of the previous sampling removals for varying parts of the decaying anatomy. To account for small differences in the size, weight, and characteristics of individual organisms (and thus produce decay indices that are more broadly applicable), we sampled 3 individuals (hereafter referred to as 'replicates') per decay species at each interval. This resulted in decaying 33 individuals of each organism, and thus 66 organisms in total. Initial wet weights of all decay organisms are given in Supplemental Material ESM2.

Upon extraction, photographs were taken of the water surface to document water surface biofilm growth. The biofilm was carefully scooped off the surface, remaining water was pipetted off, and the specimens were photographed before removal from their respective vessels. Upon exhumation from the decay vessels, tissue samples from one of the three specimens were removed for dehydration and SEM preparation. Tissue dehydration followed the protocols outlined in Nation (1983) using six successive stages of ethanol dehydration varying in concentrations from 70% ethanol to 100% ethanol, and finally hexamethyldisilazane (HMDS). The same ASW was then carefully pipetted back into the appropriate vessel after the specimen had been returned being

careful to attempt to not damage the specimens further. All three specimens were then frozen to -81°C for storage.

Ediacaran-style decay experiments.—Organisms were euthanized as before (Cameron, 2002; Nanglu et al., 2015) and then rinsed with artificial seawater to remove excess $MgCl_2*6H_2O$. Following the previous methods after euthanization, specimens were weighed, photographed, and placed in decay vessels. For these experiments, our decay vessels were 300 mL plastic rectangular storage containers; the larger sizes of these was necessitated by the more complicated nature of the experimental set-up.

Microbial mats were collected from collected from the sound side of Dauphin Island, Alabama (30°15'0.00"N/ 88°11'59.29"W), shown in Figure 2. The mat sampling locality is an estuarine tidal flat environment with medium grained, sub-angular quartz sand from dredge deposits, underlying thick (~1 cm) microbial mats. Mats that accumulate here possess a typical redox stratification of microbial types and metabolisms, indicated by a green, cyanobacteria-dominated consortium near the top, and red- to purple-colored laminae underneath, characteristic of sulfur-redox bacteria (Vasconcelos et al., 2006) (Fig. 2). Mats were collected with the top few centimeters of underlying sediment to help maintain mat integrity during the removal and transport process. We also collected organic-poor 'clean' sand from the nearshore of the sounds side of the island, to use in simulating storm deposits in the experiments. Ocean water was also collected for inoculating the ASW used in the experiments, and to supply the mats with a medium as close to their native environmental conditions as possible. After inoculation, the ASW was agitated and allowed to assimilate for 12-hours before being added to the tank that housed the microbial mats.

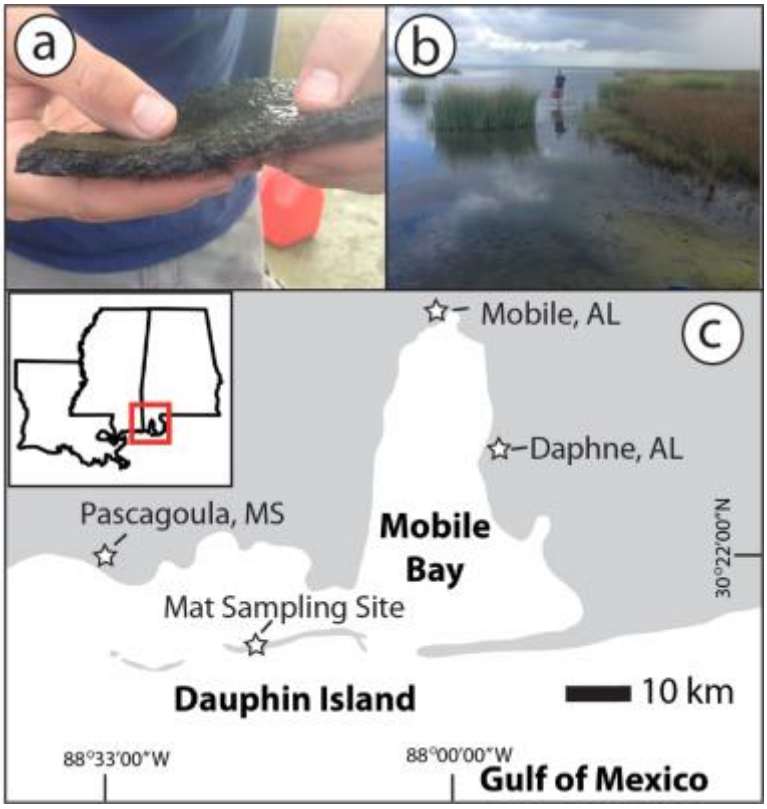

Figure 2. Microbial Mat Sampling Location Map: Location diagram of mat sampling site. (a) Image of microbial mat showing green cyanobacterial top surface. (b) Macroscopic view of mat sampling site. (c) Map showing location of sampling site on sounds side of Dauphin Island, AL, in a large tidal pool (30°15'0.00"N/ 88°11'59.29"W).

The design of Ediacaran-style experiments broadly followed that of Darroch et al. (2012), which in turn mimics the storm-burial scenario described by Gehling (1999) for the Ediacaran fossil surfaces in South Australia. A layer of sand was first placed in the bottom of the decay vessel. On top of this, we layered a section of mat (~1-2cm thick), and then placed decay specimens on top of the mat. In order to more easily split the vessels for sampling the decay specimens, sheets of plastic film (standard store-bought food wrap) were placed at the bottom of vessels as well as double layered on the tops of mats, with a circle cut out to allow contact between the decay organism and mat (see also Norris, 1989), and allow free transport of decay fluids and anions/cations around the decaying carcass. Remaining sand was then used to cover the decay specimens (~2 cm) to simulate storm deposited sediment. We saturated all decay vessels with inoculated ASW in order to prevent desiccation and better simulate a subtidal setting. Decay

vessels were then sealed using plastic film to simulate the re-growth of microbial mats over the tops of storm beds (a step not performed by Darroch et al. 2012, but nonetheless a key part of the Gehling, 1999 model).

Precambrian decay stage cataloging.— We removed three replicates per decay species from the incubator after 1, 2, 5, 8, 13, 27, 34, 41, 56, 68, and 79 days, and immediately placed in them in a -81° C freezer to simulate lithification (see Darroch et al., 2012). After freezing, experiments were cracked open along the plastic wrap seams. The organisms were examined, photographed and scored for decay state in the same characters used in baseline experiments. Any remaining tissue was then removed from the sand overlying the organism. In the event that a black precipitate was generated around the decaying carcass, this was photographed and scored as to whether it extended part-way to the edge of the decay vessel, or had filled the decay vessel entirely. Unfortunately, not all characters could be scored for each replicate due to the plastic wrap artificially biasing preservation of some characters. When plastic wrap inhibited the intersection of microbial mat and carcass, associated tissues were artificially preserved to almost pristine levels. These data were easily identified and thrown out of analyses.

2. 3 SEM EDS Analyses

All scanning electron microscopy (SEM) and integrated energy dispersive X-ray spectrometry (EDS) was conducted at the University of Missouri X-ray Microanalysis Core Facility (MizzoμX). Sediment samples were selected, generally, from up to three locations within the decay replicates: (1) proximal to the decaying organism within the black-stained sediment of the decay halo; (2) at the interface between the visible decay halo and ‘clean’ sediment; and (3) from the distal ‘clean’ sediment. The sediments were prepared for SEM-EDS analyses, comparable to the methods used by Darroch et al. (2012), by affixing extracted sediments onto carbon disc adhesive-

prepared aluminum stubs, with care taken to ensure nearly complete coverage of the adhesive. No conductive sputter-coating was applied.

Samples were analyzed using a customized Zeiss Sigma 500 VP SEM equipped with dual, co-planar Bruker XFlash 6 | 30 silicon drift detector (30 mm2 active window) EDS systems. All imaging and X-ray spectroscopic analyses were conducted with identical operating conditions: low chamber vacuum (10 Pa); 19 keV beam accelerating voltage; high current mode (40 nA probe current); 60 µm aperture; and a sample working distance of 8.5 mm. Imaging was conducted with two different detectors: a high-definition 5-segment backscattered electron detector (HDBSD; with the 4 radial segments positively biased and no bias on the 5th detector-arm segment) for compositional imaging; and a cascade current detector (C2D; with a 29.5% bias applied) for topographic imaging (measuring the resulting current from an ionization cascade). Images presented in Figure 3 represent a concurrent signal-mix from these two detectors (90:10 [HDBSD:C2D]). The EDS detectors function separately for spectral data collection, resulting in two spectra which were then averaged. At the SEM operating conditions used, the EDS detectors averaged ~15–20k counts per second, with ~20–30% dead time. Elemental mapping, with the co-planar EDS systems functioning together to provide a single map per region, was also conducted on each sample. Area spectra and elemental maps were collected from regions ~4.20 x 3.15 mm in size densely covered in sediment. Maps were typically collected from the center of the stub unless there was not adequate coverage of sediment over the carbon tape. In these instances, field of view was repositioned to the nearest area with dense coverage of sediment. Spectra were ZAF corrected and quantified using the Bruker Esprit 2 software package, with compositional results reported in normalized weight percentage. In all cases, as the majority of the carbon signal resulted from the mounting adhesive, carbon percentage was quantified but was removed prior to any post-analysis statistical calculation.

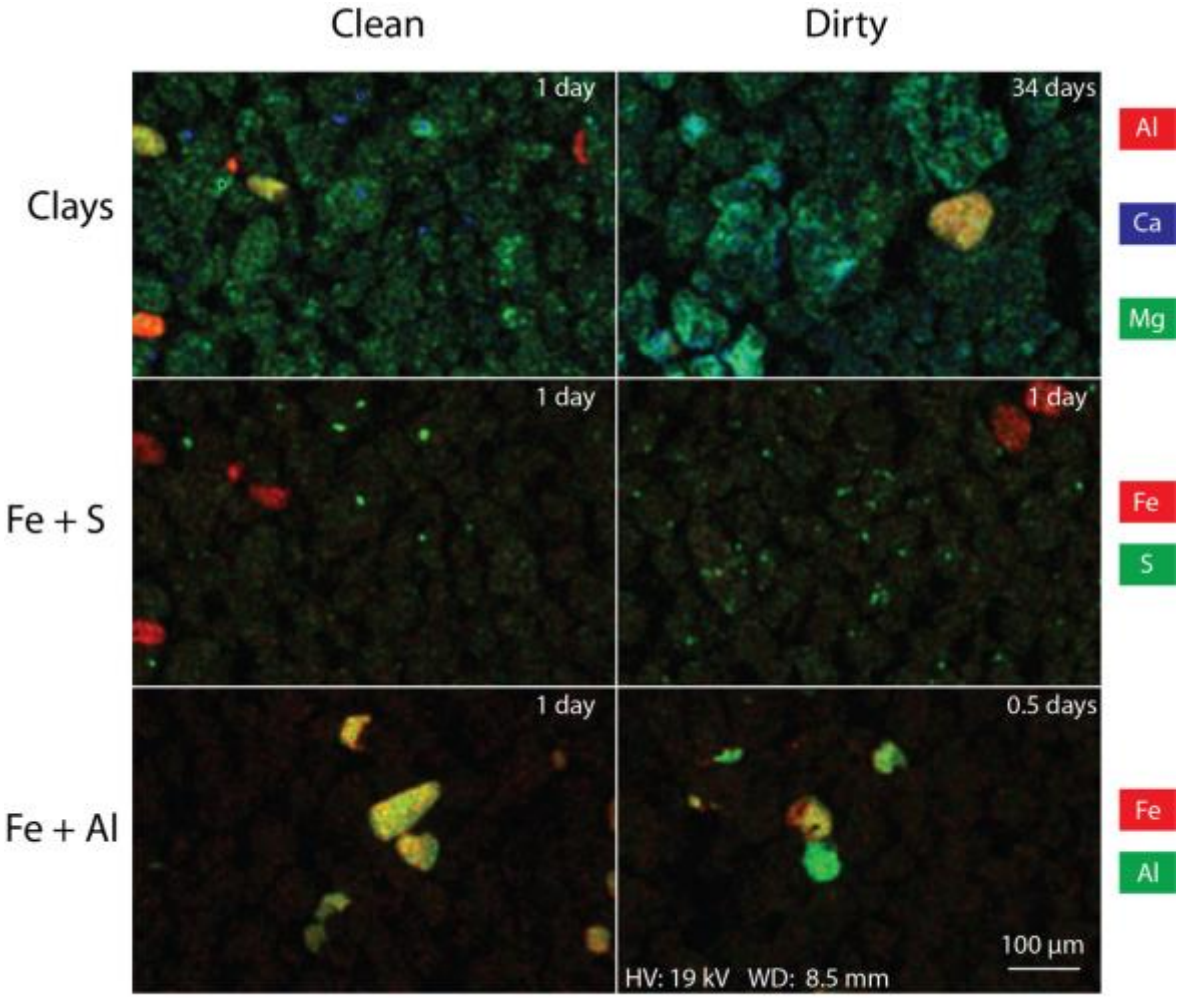

Figure 3. Elemental Mapping: Elemental mapping of sediment samples from sea hare decay experiments. “Clean” sand indicating lack of progression of decay halo into it. “Dirty” indicating black precipitate has already progressed into this sediment region.

CHAPTER 3

RESULTS

We first describe the rates and patterns of character loss in our baseline experiments; a more detailed and comprehensive list of these patterns specifically focusing on individual anatomical portions of the organisms can be found in Tables 1 and 2. We further compare and contrast these with the results of Ediacaran-style decay experiments, and finally describe the results of EDS analysis.

3.1 Baseline Decay Experiments

Condylactis gigantea (sea anemones).— Decay in sea anemones generally progressed from anterior tentacle region to posterior foot. Figure 4 shows a time series of typical progression of decay across example replicates, while Figure 5 shows the overall pattern of decay of all replicates at each time step. As shown in these figures, body tissue maintained structural integrity for the longest temporal range within the decay index, but the thickest tissues of the anemone, the foot, persisted the longest (a feature not specifically addressed by our index). Tentacles were the first character to progress out of Decay Stage 1 (‘DS1’), reaching DS2 by day 2. All other decay characters persisted in DS1 until day 5, at which point at least one replicate had transitioned to DS2. Following this pattern, tentacles were also the first tissues to progress into DS3 as well as DS4, which first occurred on days 5 and 9 respectively. DS3 was observed in replicates up until the end of the experiment, indicating that DS3 and DS4 shared significant temporal overlap among replicates. Thicker tissues such as the mesenteries (body tissue), as well as the pharynx and gametic tissues (‘gut’ tissue), progressed at a slower rate. Body tissues fully transitioned to DS2 by day 6,

and the first replicate transitioned into DS3 on day 7. Although these two events appear temporally truncated, body tissues of at least one replicate remained in DS2 upon its removal on day 18. Body tissue never actually transitioned into DS4 throughout the entire experiment, while the gut tissues only made this transition at the very end of the experiment (day 17). Though these tissues did progress into DS4, they also exhibit a similar rate of loss and DS transition history to the mesentery tissues. Outer dermal tissue decay exhibited a different rate of decay than other tissues. This tissue category remained in DS1 for a similar length of time as the 'gut' and body tissue (last occurrence on day 6), but DS2 was truncated compared to other tissues. Full transition from DS1 to DS3 took four days, and DS3 was observed even in the last set of replicates to be removed (day 18). DS4 first occurred on day 11, but some replicates did not progress to this stage by the end of the experiment.

Some aspects of the decay progression were not assessed specifically in our decay indices, but were nonetheless noted. Immediately post-mortem, the fluids in the tentacles and much of the body cavity were ejected from the organism; this caused shrinking of the organisms, but this shrinking was temporally short-lived. By the first removal of decay replicates (day 0.5), fluids had diffused back into the organisms, eliminating the shrunken character of the replicates. This is probably an artefact of the euthanizing process and left no observed permanent traces in the experiment. Furthermore, when left in the euthanizing solution, the anemones also everted a portion of their internal body cavity. This phenomenon also did not persist into the experiments and had disappeared by the first replicate removal (0.5 days). In addition, we noted that the sea anemone 'foot' was the most decay-resistant anatomical feature, although this part of the anatomy was not included in any of our scored characters. Lastly, the carcasses varied in density throughout the decay window. Although initially at the base of the vessels, the carcasses became more positively buoyant for a temporary amount of time before returning to negative buoyancy and resting at the base of the vessels again. This usually occurred at day 3 and day 12 for positive and negative buoyancy, respectively.

Table 1 Sea Anemone Morphological Character Decay

Character (decay bin)	Description	Decay Index Pattern of decay	Ediacaran-style decay pattern
Tentacles (anterior region)	Thin fluid-filled sacks used for stinging food	Rapidly lost	Rapidly lost, often turns into diffuse blob off tissue
Mesenteries (body tissue)	Longitudinal tissue that fully or partially connects to pharynx tissue	Most resistant to decay	Most resistant to decay
Outer-most dermis (outer dermal)	This layering of cells that usually appears clear above colored tissue around body	Initially turns vitreous, then sloughs off	Often diffuses into surrounding sediment, altering the coloration of the sediment
Foot (outer dermis/body tissue)	Thickest portion of the organism; provides structural support for attachment	Thickest, most cohesive tissue, persists	Often folded over itself, but also most likely to persist
Pharynx (gut)	Folded endodermis that attaches to the oral opening	Rapidly becomes less consolidated, but tissue material persists	Similar to Index Pattern, but maintains form for a much longer period of time
Gametic tissue (gut)	Internal, located near the foot	Rapidly lost, turns into diffuse liquid	Similar to pharynx, form is lost as diffuses into liquid

Table 2 Sea Hare Morphological Character Decay

Character (decay bin)	Description	Decay Index Pattern of decay	Ediacaran-style pattern of decay
Rhinopores (anterior)	Appendages of the head for sensory	Typically persists almost as long as overall out dermis	Often persists for as long as anterior region is present
Head (anterior)	Small portion of the body that houses the mouth and radula	As decays, it begins to tear and diffuse easily as compared to rest of carcass	Maintains structure much longer than basline
Siphonal flap ()	Opening to internal anatomy, used for locomotion by moving water through	Opens as carcass bloats, then closes after gas is lost	Feature appears to be lost under Ediacaran conditions
Gill (gut)	Internal tissue protected by posterior shell; used for oxygen consumption	Rapidly is lost as turns to black sludge	Same pattern as baseline, but much slower rate
Longitudinal muscle (body tissue)	Used for locomotion, thicker tissues		
Organs and glands (gut)	Used for reproduction and other physiological processes	Rapidly is lost as turns to black sludge along with gill	Same pattern as baseline, but much slower rate
Dermis (outer dermal)	Epidermis tissue that surrounds the organism	Typically persists after internal features have decayed	Typically decayed from ventral to dorsal, possibly due to position on mat

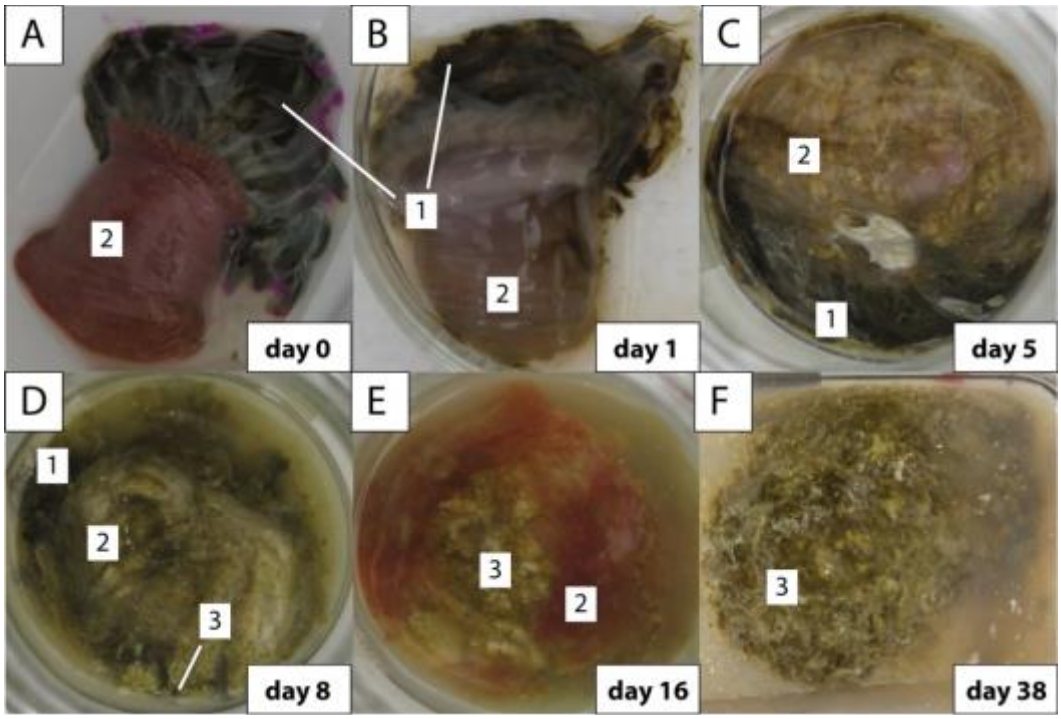

Figure 4. Progression of Baseline Sea Anemone Decay: Progression of decay for giant sea anemone, *Condylactis gigantea*, under baseline conditions. (1) tentacles, (2) body column, (3) 'gut' material contracting and decaying from outer dermal layer, (4) sludge buildup from underneath posterior plate.

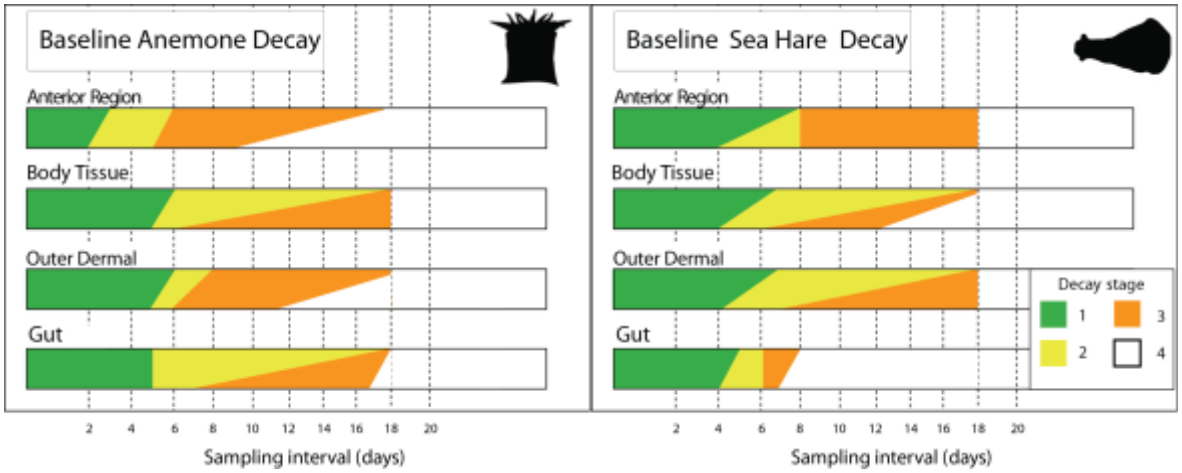

Figure 5.Baseline Decay Rates and Patters: Pattern and temporal range of baseline-condition decay assessed from generalized decay characters. Left side shows relative decay patterns for *Condylactis gigantea*, and right side shows *Dolabella auricularia*. Colors indicate first and last observation of decay stag, such as Decay Stage 1 (DS1, green) indicates 0-25% loss of the decay character (e.g. "anterior region", " body tissue", etc.), DS2 indicates 25-50% loss, etc.

Dolabella auricularia (opisthobranch gastropods).— Decay in the sea hares generally progressed outward from the carcass starting in the 'gut' (Fig. 5). Outer dermal tissues became translucent (Fig. 6) as the experiment progressed, and internal 'gut' tissues as well as internal tissues of the head darkened throughout decay. This was most evident by the end of the experiment as shown in day 18 of Figure 6F. All characters in *D. auricularia* persisted in DS1 until day 4, at which time all tissue regions in at least one replicate transitioned into DS2 (Fig. 4). That is not to say that the same replicate transitioned entirely into DS2 for all of its individually measured characters, rather transitions were staggered across replicates. Unlike the tentacle region in sea anemone experiments, the anterior region of the sea hares did not deteriorate more rapidly than the other tissues. The anterior region of the sea hares progressed through DS2 at the same pace as other tissues and stayed in DS3 for the remainder of the experiment. During DS3, rhinopores were no longer individually discernable, but the overall outline of the morphology was conserved (Fig. 6). The tissues of this region transitioned to DS3 by day 8 and remained in DS3 until the end of the experiment. A similar pattern occurred with the outer dermal tissues, which persisted in DS2 and DS3 from day 4 until the end of the experiment. The gut tissues of the sea hares, which consisted of the opaline gland, gill, and purple gland, was entirely lost by all specimens early on in the experiment. By day 8 all evidence of these parts had been replaced by a black sludge typically located underneath the stiffened posterior plate (Fig. 6F). In the last set of replicates (day 18), two of the three experiments had progressed to DS4 with respect to the 'muscle' (see Methods, Comparative anatomy and construction of decay indices).

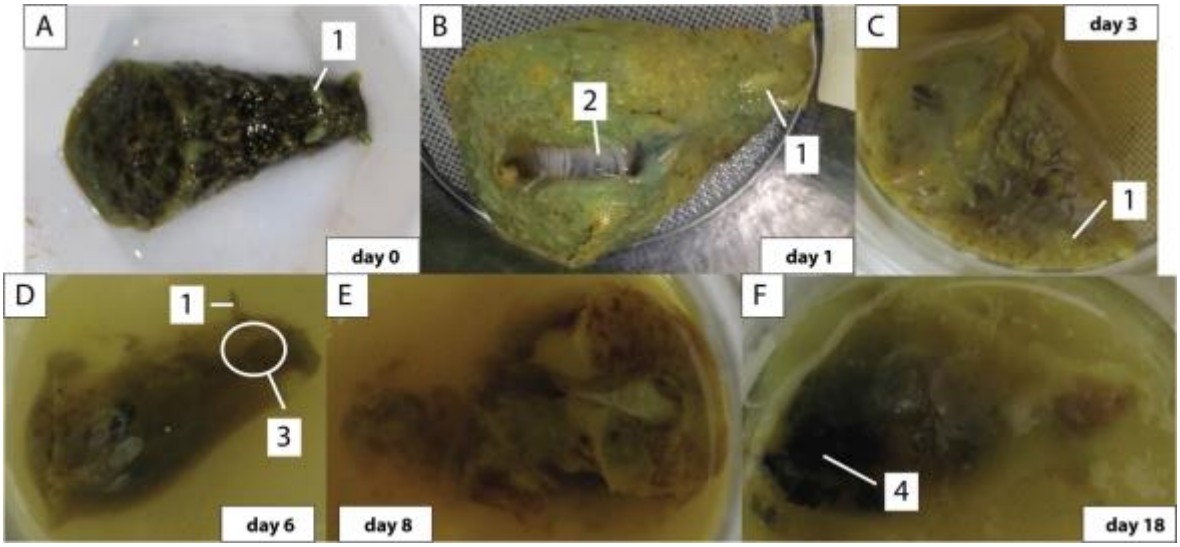

Figure 6. Progression of Baseline Sea Hare Decay: Progression of decay for wedge sea hare, *Dolabella auricularia*, under baseline conditions. Labeled characters: (1) rhinopores, (2) calcareous shell, (3) gut leaching out becoming too decayed to discern further.

As with before, some aspects of the decay experiments were not captured by our decay indices. Specifically, sea hares bloated early in the decay progression. This was most noticeable along the siphonal flap on the dorsal posterior portion of the organism. During bloating the interior body cavity of the organism was readily exposed showing the gill and the calcareous shell (Fig. 6B). As decay progressed, bloating of the carcass decreased which was most noticeable by the siphonal flap closing, no longer leaving the internal anatomy exposed.

Figure 7 illustrates these patterns of decay for both sea anemones and sea hares in a more visually-comprehensive way. These two taxon summaries are simplified to allow for easy comparison to extinct fossils.

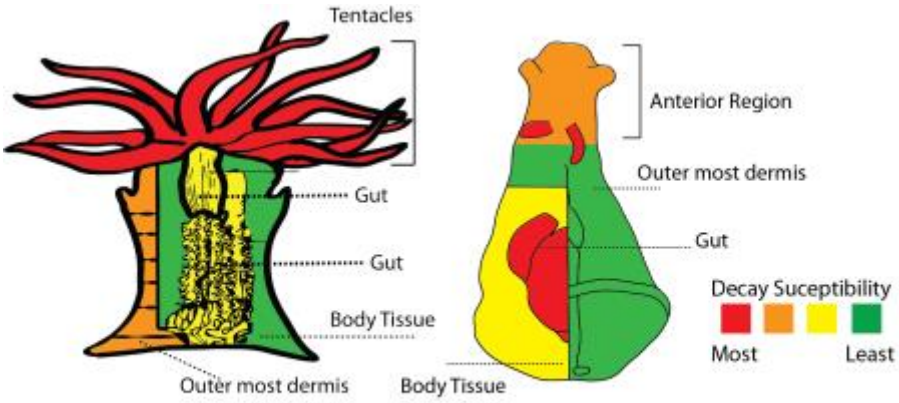

Figure 7. Decay Indices: Decay indices for *Condylactis gigantea* (left) and *Dolabella auricularia* (right). Colors correspond to least susceptible to decay to most susceptible (e.g. green = least susceptible, yellow = susceptible, orange = more susceptible, and red = most susceptible).

3.2 Ediacaran-style Decay Experiments

Condylactis gigantea (sea anemones).— The pattern of character loss for sea anemones under Ediacaran-style death mask conditions (Fig. 8, Fig. 9) was very similar to that seen in baseline experiments (Fig. 4, Fig. 5). The rank of most decay-susceptible tissue to least decay-susceptible tissue was: the anterior region (tentacles), gut tissue (gametic and pharynx tissue), outer dermal tissue, and body (mesentery) tissue. In the baseline experiments, the outer dermal tissue was more susceptible to decay than the gut tissue, which is reversed in the Ediacaran-analogue experiments. This reversed pattern should be accepted cautiously, though, because compaction of the organism during decay made assigning DS values to the internal tissues difficult at best. Furthermore, DS values for the gut tissues and dermal tissues are very similar, with both tissue types exhibiting DS3 values for much of the experiment (days 8-68 and days 5-68, respectively).

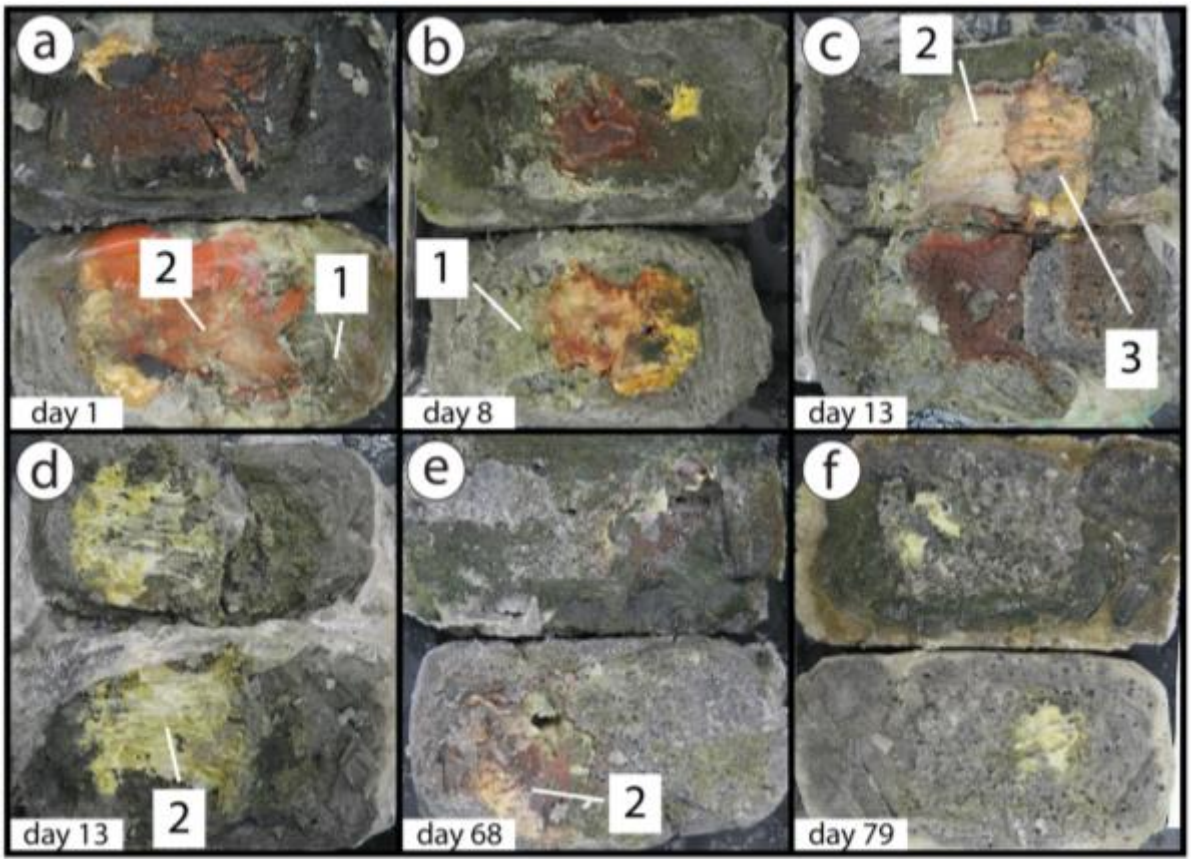

Figure 8. Progression of Ediacaran-style Sea Anemone Decay: Progression of decay for giant sea anemone, *Condylactis gigantea*, under Ediacaran-style decay conditions. Labeled characters: (1) remains of tentacles, (2) remains of body muscle.

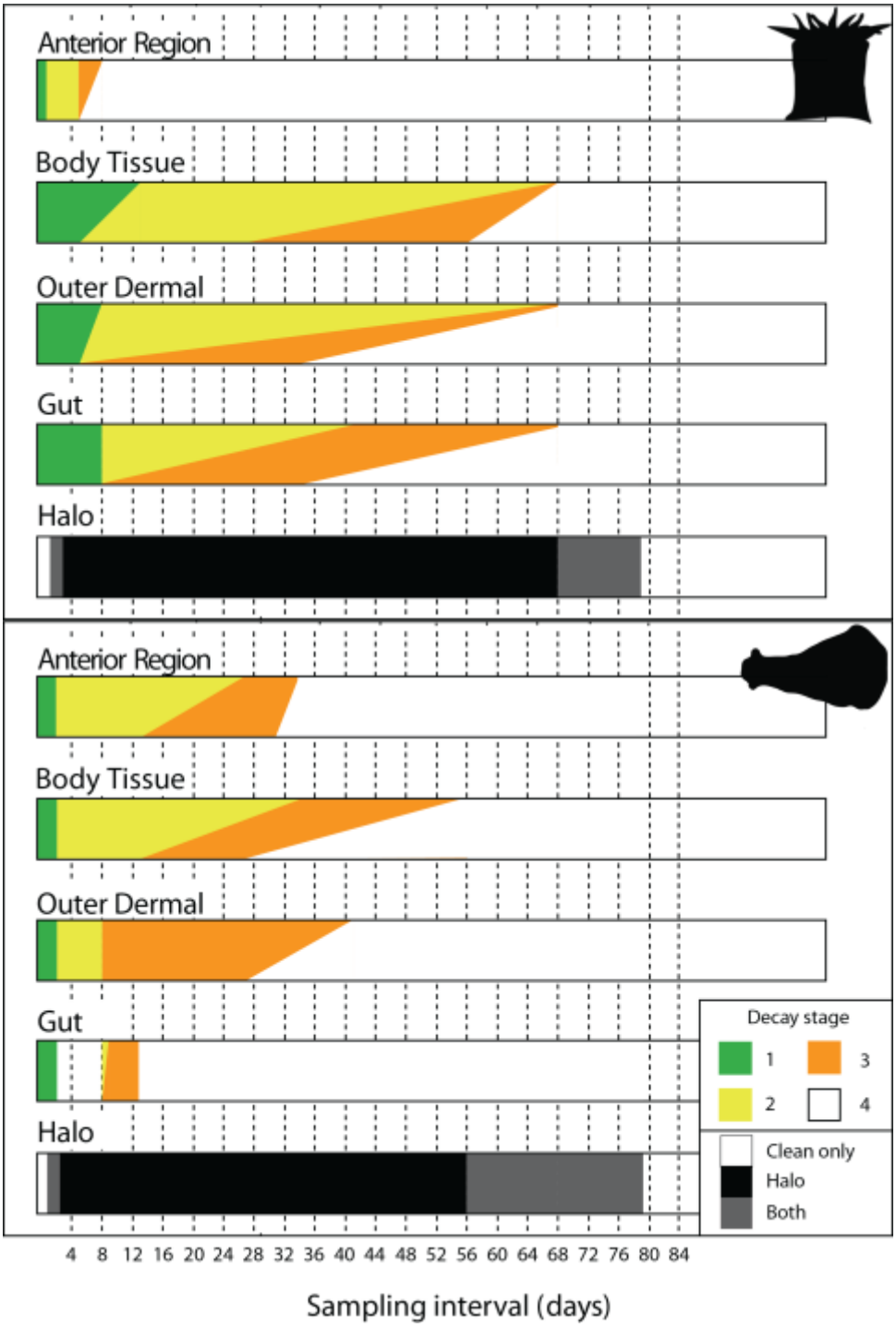

Figure 9. Ediacaran-style Decay Rates and Patterns: Pattern and temporal range of Ediacaran-style decay assessed from generalized decay characters. Top shows relative decay patterns for *Condylactis gigantea*, and bottom shows *Dolabella auricularia*. Colors indicate first and last observation of decay stag, such as Decay Stage 1 (DS1, green) indicates 0-25% loss of the decay character (e.g. "tentacles", "gut", etc.), DS2 indicates 25-50% loss, etc. Sea hare gut experiences a gap in data between DS1 and DS2 due to non-recoverable samples.

Although patterns of decay were very similar, decay rates were vastly different between the baseline and Ediacaran-analogue experiments. For the most part, Ediacaran-analogue experiment tissues transitioned into subsequent decay stages at a much slower rate than those under baseline conditions. Counter to this broad trend, the tentacles (anterior region) persisted for less time under Ediacaran conditions than the baseline conditions (last observation of DS on day 9 and 17, respectively). Although this increased decay rate of the tentacles was counter to the overall delayed Ediacaran-type rate, the overall pattern of the thinnest, most labile tissues being lost first was consistent across the baseline and Ediacaran-style decay experiments.

As before, some aspects of the baseline decay experiments were not directly assessed in the decay indices. The foot of the sea anemones was again the most resistant feature to decay. This was further compounded by the additional factor of the tissues of the foot (1) folding over on itself and reducing exposed surface area, and (2) having the additional structural support provided by the surrounding sediment. This structural support reduced the amount of stress on the tissues for falling apart. In the baseline experiments, the sea anemone carcasses maintained neutral to just negative buoyancy. As the replicates did not rest on the bottom of the vessels during these experiments, they did not maintain shape as well during the decay processes. In these Ediacaran experiments, while the body tissues persisted, they maintained shape much better than the baseline experiments. This trend is most evident in the foot and fairly evident in the body tissues, though it should be noted that this may partially be affected by the folding over of tissue on itself in this region.

Dolabella auricularia (opisthobranch moolluscs).— In the same manner as *C. gigantea*, the pattern of character loss in *D. auricularia* under Ediacaran-style death mask conditions (Fig. 9, 10) was very similar to that exhibited in baseline experiments (Fig. 5). The rank of most decay-susceptible tissue to least decay-susceptible tissue was: the gut tissue, the outer dermal tissue, the anterior region (head), and the muscle. The most notable difference in patterns between these two experiments was seen in the outer dermal layer was much more susceptible to decay under Ediacaran-style conditions.

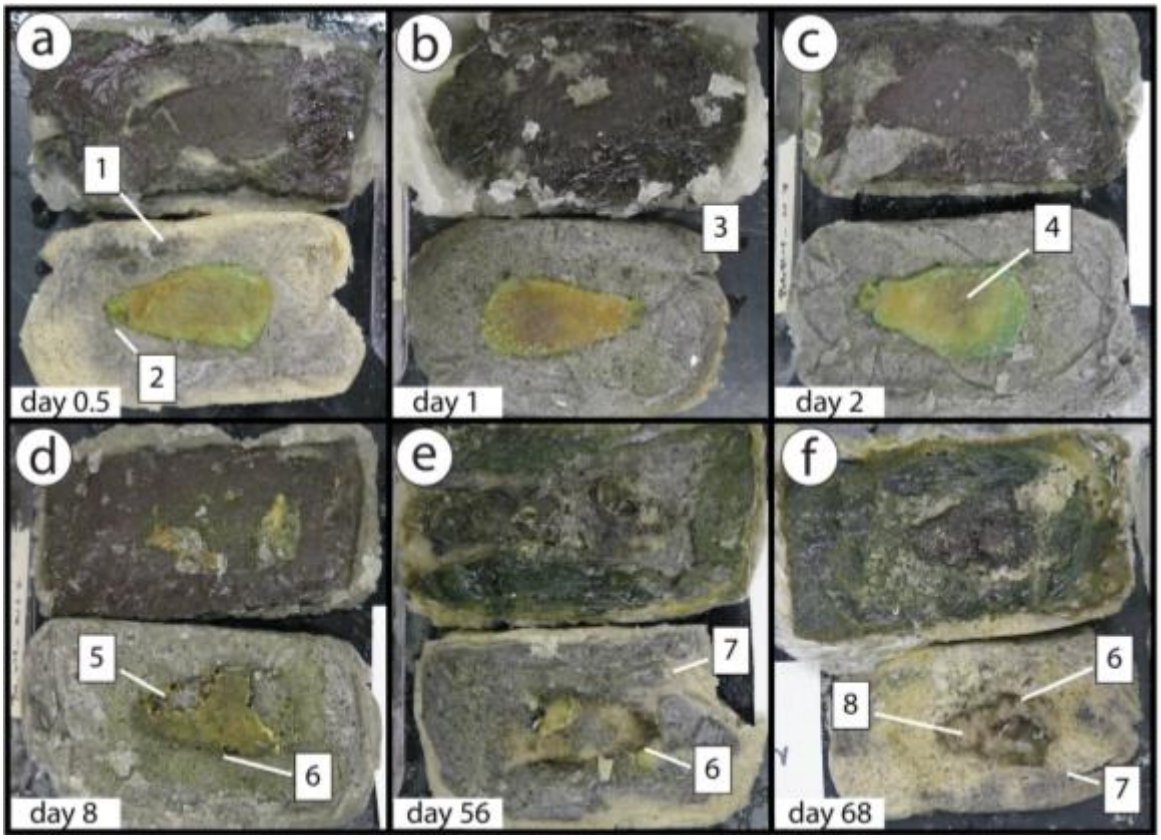

Figure 10. Progression of Ediacaran-style Sea Hare Decay: Progression of decay for wedge sea hare, *Dolabella auricularia*, under Ediacaran-style decay conditions. Labeled characters: (1) Emergence of decay 'halo' black precipitate, (2) anterior portion (head), (3) Black precipitate halo encompassed decay vessel entirely, (4) discoloration from internal gut decay, (5) internal gut mostly removed with persistence of outer dermal layer and muscle, (6) outline of carcass persists, (7) decay halo begins to retract, (8) cavity where carcass has entirely decayed.

Under baseline conditions, the outer dermal layer was still present even at the end of the experiment, while under Ediacaran conditions this tissue layer appeared to diffuse into the surrounding sediment beginning on day 8 and was entirely lost by day 41. Breaking down the patterns by character, the muscle and dermal tissues persisted in DS3 for the majority of the experiment (days 13-56 and days 8-41, respectively). Sea hare muscle exhibited DS2 for a longer period than sea hare outer dermal tissue (days 2-35 and days 2-8, respectively). Lastly, the pattern of tissue loss for the anterior region of the sea anemone replicates was fairly mixed between that patterns for the muscle and dermal tissues. Replicates spent ca. equal time in DS2 and DS3 (days 2-

27 and days 13-34, respectively) before transitioning entirely into DS4 on day 41(where it remained for the rest of the experiment).

Similar to the sea anemones, *D. auricularia* decay rates were drastically slower than in baseline experiments. All characters transitioned into DS2 by day 9, and body tissues and anterior tissues did not fully transition into DS3 until day 36 (meaning DS2 was still noted in at least one replicate up until this point). The last reported DS3 values for the body tissues and dermal tissues were days 56 and 41, respectively.

Black decay 'halos'.— In all replicates for both *C. gigantea* and *D. auricularia*, a black 'halo' precipitated on the surface of the sediments surrounding the carcass, similar to that noted in Darroch et al. (2012). The development and progression of these halos across replicates is shown in Figure 9. Decay halos appear at the start of experiments, after 12-hours in both organisms. By day 9, halos had entirely encompassed all of the decay vessels with no 'clean' sand visible. This progression occurred contemporaneously in both the sea anemones and sea hares. Halos persisted until the end of the experiment, at which point there was some contraction towards the carcasses in a few replicates, although no vessel entirely lost visible signs of the black precipitate.

To assess the composition of this precipitate and its importance in 'death mask' style preservation, multiple sediment samples were scanned from each decay vessel to track any changes that occurred throughout the temporal range of the experiment. The relative elemental mass abundances for each of these samples is shown in Supplemental ESM3. Figure 11 shows the progression of Fe, S, Al, Mg, and Ca throughout the experiment, as well as tracking the changes in each of these abundances by location of sediment sample.

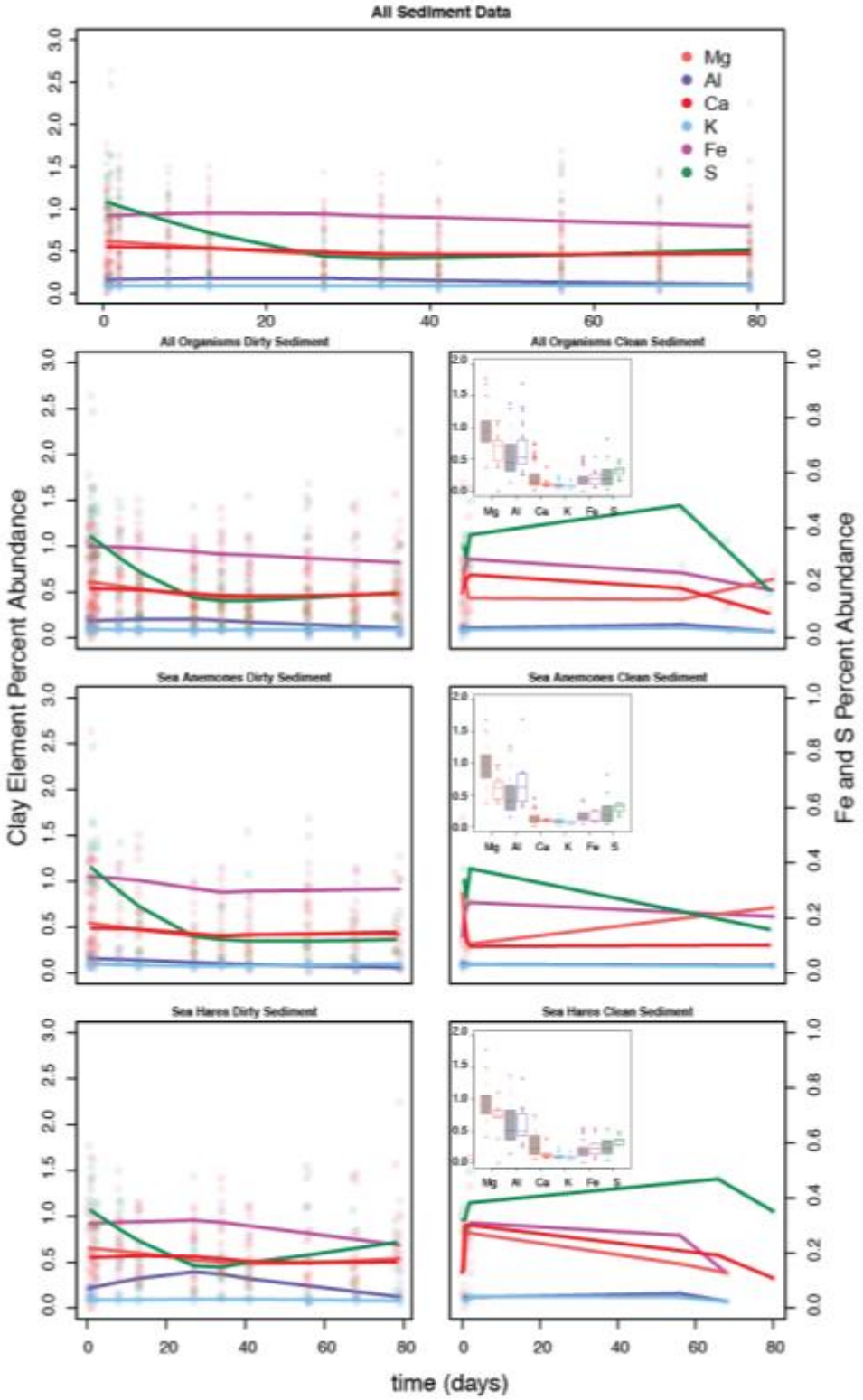

Figure 11. Elemental Abundances of Decay Sediments: Elemental abundances of "clean" and "dirty" sediment from the decay vessels (e.g. sediment outside or within the decay halo, respectively). Boxplots show comparisons between "clean" (gray) and "dirty" (white) sediments for individual elements. Elements displayed are Fe (red), S (green), Mg (purple), K (light blue), Al (pink), and Ca (dark blue). Fe and S are plotted on secondary y-axis.

3.3 SEM EDS Analyses

Sediment samples (n = 147) were analyzed from the 66 decay replicates used in Ediacaran-style decay experiments. 'Clean' sediment from prior to the onset of the decay experiments indicated a dominantly siliceous composition with abundant Mg, low K, and low Na. The enrichment of Mg was most likely due in part to the high Mg-concentrations of the AWS used to saturate the decay vessels for the duration of the experiment. Elemental mapping of sediments collected from the decay halo (Supplemental Material ESM3) revealed the presence of C, O, Na, Al, Si, S, Cl, K, and Ca in all sediment samples, and Mg present in all but one sediment sample. Elemental mapping also revealed Fe present in all but two samples. Ti was only present in twenty samples.

We analyzed our sediment samples in bins based on location of excavation in relation to the carcass and the decay precipitate halo front. Sediment samples were broken down into four groups for each organism type: (1) decay halo sediment proximal to the carcass, (2) sediment from the intersection of the halo and the 'clean' sand, (3) sediment that was entirely from 'clean' sand outside of the decay halo, and (4) sediment excavated from near the edge of the vessel when decay halos encompassed all of the sediment within their vessels. The abundances of different elements are expressed as percentages, which reflect the amount of each element observed in each elemental map where the sum of all observed elements equals 100%. These data are shown in Figure 11 and Supplemental Material ESM3.

Decay halo.— Sea anemone S started out high (c. 0.55%; though one replicate anomalously c. 0.82%) early in the experiment, and rapidly decreased to a typical range of ~0.05 – 0.25% for the rest of the experiment. Sea hare S followed a similar pattern, though there was more variation in later decay replicates (and no anomalously high recorded value early in early replicate). K levels

remained fairly consistent throughout the experiment with levels ranging from ~0.03 - 0.20% and ~0.04 - 0.25% in sea anemones and sea hares, respectively. Ca levels in the sea anemone sediments were low, with all values beneath 0.45% and most values beneath 0.20% for all 79 days. Ca levels in the sea hares were more variable and more elevated than the sea anemones. Ca values in sea hares were as high as ~0.75%, though most values were around the range of sea anemones (e.g. 0.15 - 0.60%). Mg and Al levels were the highest values as well as most variable in both decay species. In sea anemones, Mg sediment values ranged from ~0.36 – 2.63%. Al levels ranged from ~0.18 – 1.27%. Sea hare values for these ranged from ~0.41 - 1.77% and ~0.13 – 1.29% for Mg and Al, respectively. Fe was variable throughout the experiment with most values ranging between ~0.05 – 0.3% and ~0.08 – 0.4% for sea anemones and sea hares, respectively.

In terms of changing elemental compositions through time, in both sea anemones and sea hares Mg appears to decrease over the duration of the experiment. Ca exhibits relatively little change in sea anemone replicates, but it follows a more sinusoidal pattern in sea hares. In both sea anemones and sea hares, Al initially decreases, but then increases towards the end of the experiment. Fe follows the same pattern as Al for both decay organisms, but S experiences a large decrease and only subsequently increases slightly as compared to the magnitude of the initial decrease.

Sediment stub elemental maps show very little spatial co-occurrence of Fe and S, although S ‘hot spots’ are observed in much of the sea anemone ‘clean’ sediment, and occasionally in the decay halo sediment of the anemones. Additionally, Fe and Al regularly exhibit a spatial association (shown in Fig. 3), as do Ca and Mg as well as Ca and Al. This association, which is typically found on specific grains with the sample, is very rarely widespread over the entire map. This occurs more consistently with the sea hares than with the sea anemones.

Intersection between ‘halo’ and clean sediment.— Because of the progression of the halo and eventual encompassment of the decay vessel, there are less data for this sediment boundary. Only three time-steps (days 0.5, 1 and 79—a post-retraction boundary) for sea anemones and two

time-steps (days 0.5 and 1) for sea hares had this sediment boundary at sampling time. In all elemental maps, the same trends as in the decay halo sediment data appear. Furthermore, in the sea anemones there appears to be a decline in all elements from the beginning of the experiment to the final time step. That being said, the day 79 sea anemone data are based off of a single replicate.

Vessel edge.— For the majority of the experiment, the decay halos had expanded to encompass their entire respective vessels. In both sea anemones and sea hares, S values ranged from ~0.04-0.50%. Iron levels were lower in the sea anemone sediments, with values ranging from ~0.05-0.31%. In sea hare sediment, iron levels ranged from ~0.06-0.52%. Clay elements exhibited much of the same pattern that they did in the decay halo sediments, with there being relatively little K (sea anemones ~0.01 – 0.19%; sea hares ~0.05 – 0.15%), low Ca in the sea anemone sediments (~0.01 – 0.26%), higher Ca in the sea hare sediments (~0.07 – 0.50%), and large variations of Al concentrations in both sea anemone and sea hare sediments (~0.15 – 0.89 and 0.24 – 2.25, respectively). Mg levels were also typically high for both species but also had highly variable values (~0.51 – 1.33% and ~0.47 – 1.14%, respectively).

'Clean' sediment.— Similar to the 'clean' and decay halo intersection sediment, fewer replicates had 'clean' sand preserved due to the rapid precipitation of the decay halo. With the anemones, the only 'clean' sand occurred at the beginning of the experiment (days 0.5 and 1) and right at the very end of the experiment (day 79). Occurrence of 'clean' sand in the sea hare portion of the experiment was a bit more complicated. Replicates at the beginning for the experiment had 'clean' sand for the same period as the anemones, but the later replicates were more variable in which ones had 'clean' sand. Two time-steps each had a single replicate with clean sand (days 56 and 68). In all cases with the exception of K and S, there was a general decrease in concentrations of clay elements and iron sulfide elements from the early replicates to the later replicates (Fig. 11).

In summary, although elemental abundances were highly variable throughout the temporal range of the experiment, several patterns did emerge. Firstly, elemental abundances for silicon and oxygen remained fairly constant throughout the experiment duration. Secondly, there is very little

in the way of spatial association or percentage of coverage between iron and sulfur within the decay halo; sulfur in the decay halo around both species experienced a large decrease shortly after the start of the experiment, and never recovered to previous levels. Furthermore, there were no observed occurrences of overlapping Fe and S in the elemental maps. Thirdly, some cations do appear to overlap on some sediment grains in the elemental maps, the most notable of these associations was between Fe and Al.

Lastly, some differences emerged between the 'clean' and 'dirty' sediments (i.e., those within and outside of the decay halo). 'Clean' sediment consistently exhibited lower abundances in mapped elements, especially S. Fe was always lower in the 'clean' sand at the end of the experiment, when clean sand was present. Counter to this, S was typically at a higher concentration in the 'clean' sediments when 'clean' sand was present later in the experiment. Sediment sampled from the intersection of 'clean' and dirty sediment always returned elemental abundances within the ranges of 'dirty' sediment from the decay halos.

CHAPTER 4

DISCUSSION

We first address the original five questions listed in the introduction, and then discuss the broader implications of our data for both Ediacaran taphonomy, and their utility for potentially reinterpreting Ediacaran fossils.

4.1 Original Five Questions

Do Ediacaran-style taphonomic scenarios affect the 'normal' (i.e., open marine) pattern and rate of decay?.— Patterns of decay were almost identical between baseline decay experiments and the Ediacaran-style decay experiments in both organisms. The notable exceptions to this were observed with respect to the 'outer dermal' and 'gut' characters. In the baseline experiments, the outer dermal layer in sea anemones was more susceptible to decay than the 'gut' character, but under Ediacaran-style conditions, this character became less susceptible, and persisted longer than the 'gut'. This reversal in the relative susceptibility of this character was also seen in the sea hares; the outer dermal layer in this organism was more susceptible to decay in the Ediacaran-style conditions than the baseline conditions. However, in Ediacaran-style conditions, the 'gut' of the sea hare decayed more quickly than the outer dermal layer, particularly the transition from DS3 to DS4. The fact that the outer dermal layer persisted longer than the 'gut' in Ediacaran-style experiments, in both anemones and sea hares, has important implications for the interpretation of Ediacaran fossils (discussed below).

Although patterns of decay were broadly similar in the two experiments, rates of decay were much slower in Ediacaran-style experiments than in baseline experiments (Fig. 5, 8). In both sea anemones and sea hares, the least structurally complex tissues were the first to transition from

early decay stages to later decay stages. The tentacles of the sea anemones are the thinnest tissues of either decay organism, and in both experiments this character was lost more rapidly than any other character with the exception of the 'gut' in the sea hares. The rapid decay of tentacles is likely due to their tissue structure; as fluid-filled sacs with large surface area, these tissues intuitively decompose more readily than thicker, less labile tissues such as the thick body tissues of the anemones. Counter to what we expected, the tentacles in baseline experiments persisted longer than those subjected to the Ediacaran-style conditions. This is plausibly a result of the large starting consortium of bacteria present in the microbial mats that could facilitate early decay. This observation has implications when interpreting fossils that might have a cnidarian- or actinian-affinity (for example, in the Ediacaran) - as tentacles are more susceptible to being lost in Ediacaran-style taphonomic scenarios, there is a strong possibility that they are under-represented in Ediacaran fossil deposits (as compared deposits such as Mazon Creek which preserve tentacles), thus hindering fossil interpretation, and robbing paleontologists of valuable anatomical and ecological information.

Do equivalent FeS 'death masks' form with both triploblastic and diploblastic organisms?.— In our Ediacaran-style experiments, there was little evidence to support FeS 'death masks' forming in either our diploblastic or triploblastic decay organisms. Although we did see slower decay under Ediacaran-style conditions, we did not observe a spatial association between Fe and S in the EDS data (Fig. 11), in stark contrast to the experiments performed by Darroch et al. (2012). This could be attributed to a couple of reasons. Firstly, our sediments were low in Fe, which may in turn imply that 'death mask' style preservation is reliant on a minimum level of iron in sediments, and that sediments with higher concentrations of Fe will produce better 'death masks' and (presumably) higher fidelity preservation. Counter to this argument is that Ediacaran fossils have been reported from carbonate sections in China (Chen et al., 2014), implying that high Fe is not strictly necessary for forming death masks. In contrast, it is unlikely that the limiting reagent

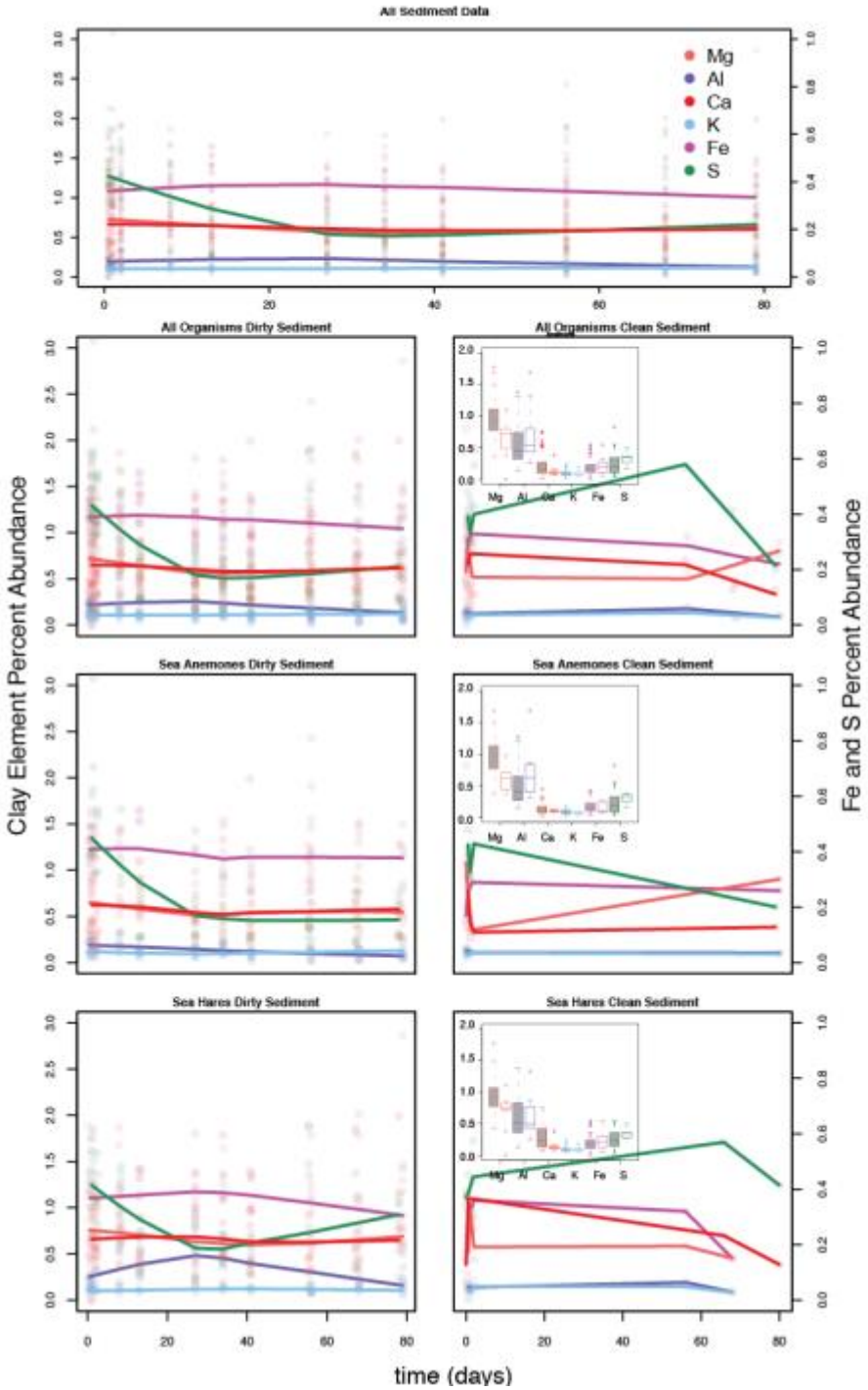

Figure 12. Elemental Abundances of Decay Sediments Normalized to C: Elemental abundances of "clean" and "dirty" sediment from the decay vessels (e.g. sediment outside or within the decay halo, respectively) renormalized with carbon removed. Boxplots show comparisons between "clean" (gray) and "dirty" (white) sediments for individual elements. Elements displayed are Fe (red), S (green), Mg (purple), K (light blue), Al (pink), and Ca (dark blue). Fe and S are plotted on secondary y-axis.

in our experiment was S. Ediacaran seawater is thought to have had sulfate levels up to two orders of magnitude lower than at present (Hayes et al., 1992; Canfield, 1998; Shen et al., 2002; Shen et al., 2003; Poulton et al., 2004; Shen et al., 2008), which is not reflected in our use of Instant Ocean artificial seawater to saturate experiments.

Another possible explanation for the lack of FeS 'death mask' formation observed in our experiments (and in contrast to that seen in Darroch et al., 2012), is that our experiments use decay organisms lacking rigid exoskeletal tissues. Darroch et al. (2012) used waxworms (*G. mellonella*) which have a relatively thick chitinous cuticle, whereas our decay organisms (sea anemones and opisthobranch mollusks) lack such structurally rigidity. If we assume that tissues with greater strength and rigidity (especially those with cross-linked polysaccharides) are more recalcitrant, then slower decay and maintenance of localized anoxia around the decaying carcass would be a key to 'death mask formation'. This in turn would indicate that most, if not all, of the Ediacara biota would possess a stiffened, perhaps even chitinous cuticle. However, we think this is unlikely, given the evidence to the contrary, such as the range of in degrees of complexity of associated with the Ediacara biota. Organisms such as *Funisia*, whose structure and aggregative associations have been attributed to close relations to cnidarians or sponges, appear much less rigid than those such as *Kimberella*, which might have had a lightly biomineralizing carapace (Droser and Gehling, 2008). Perhaps a more likely explanation, albeit not a new one, would be that the structural rigidity of some tissues during this time could have existed in a form that was also easily degradable though still robust, such as collagen or chitin (Towe, 1970; Meyer et al., 2014). Decay experiments using a broader range of invertebrate taxa are needed to test this idea in further detail, though.

Are the dark decay 'halos' consistently associated with the precipitation of aluminosilicate elements?.— Darroch et al. (2012) noted a higher concentration of aluminosilicate elements within black decay 'halos' around decaying *G. mellonella* larvae than within the 'clean' sand outside it, and used this to suggest that authigenic clay mineral formation (which would effectively mold the

external morphology of the carcass, as well as create an impermeable barrier preventing diffusion oxygenated pore fluids) may have be an important component of Ediacaran preservation. Although our decay EDS data are more variable, we note increased Al concentrations in decay 'halos' around carcasses, once carbon is removed (Fig. 12). Although removing carbon and re-normalizing adds more noise, stronger patterns associated with elements with lower abundance percentages begin to emerge. Specifically, Al typically fluctuates a bit more for the duration of the experiment, and it begins to increase in concentration towards the end (Fig. 12). That being said, these increases and fluctuations are not substantial enough to definitively state that aluminosilicate precipitation is high in the vicinity of the carcasses (i.e., within the halos), relative to 'clean' sand.

What is the rate and pattern of aluminosilicate precipitation as decay progresses?.— When carbon is removed from the data and the data re-normalized, Al (as a proxy for bulk aluminosilicate) abundance initially decreases inside the decay halo in all samples, and then subsequently increases. This increase is not persistent in all sediment bins, as no increase is noted from sediment collected from the edge of the decay vessel during which the decay halo had completely encompassed the vessel in the anemone experiments (Fig. 12). The percentage coverage of K and Ca remain fairly constant throughout, with K maintaining almost 0% for the entire duration of the experiment. The only noticeable spatial association in EDS maps are between Fe, Al, and between Al and Ca. In sea hares, Al and Ca clump more than they do with anemones. This is likely due to the local enrichment of calcium from the posterior shell.

What is the relative importance of FeS vs. clay minerals in molding the external morphology of carcasses, and thus in fossil preservation?.— When looking for clay element co-occurrences in the EDS spatial maps, there is a greater degree of spatial association between aluminosilicate elements than observed with the Fe and S maps, but still not enough to suggest the formation of clay minerals. More interesting is the tight association of Fe and Al, which often

overlap (Fig. 3). Fe more often occurs on sediment grains that have Al, than it does for areas of increased S. Previous work has demonstrated that biofilms (which typically have negatively charged surfaces) may be attract positively charged elements (Ferris et al., 1989). It conceivable that areas with increased Al in our sediment samples correspond to areas of increased biofilm production, something not specifically analyzed within this project. If this is demonstrated to be true, then Al an Fe association could potentially be used as a proxy for biofilm production, but this should be tested much more rigorously before being used as such.

4.2 Broader Impacts

The results of these experiments have implications both for the interpretation of Ediacaran fossils, as well as the efficacy of the pyritic 'death mask' model for Ediacaran fossil preservation. For interpreting Ediacaran fossils, the observation that the decay of key characters (the tentacles of sea anemones, and the 'guts' of both sea hares in particular) are not significantly slowed in Ediacaran-style taphonomic scenarios (and in some cases, decay even faster than in baseline 'open' conditions), suggests that these characters are unlikely to be recognized in Precambrian fossil assemblages, even if they were present. In other words, our experiments thus show that Ediacaran 'death mask' conditions bias against key actinian and molluscan characters that would typically be used to constrain the phylogenetic affinity of fossils. More specifically, the rapid decay of tentacles in our sea anemone experiments illustrates that Ediacaran preservational pathways may confound reliable interpretation of fossils as actinian-grade cnidarians Although developed with Ediacaran preservation in mind, our indices can be used to investigate different preservational modes of primarily soft-bodied taxa. We tested the usefulness our or indices and comparative decay patterns outside the Ediacaran by looking at the Cambrian organisms *Mackenzia*. This fossil has been interpreted as an anemone of the earliest Phanerozoic (Conway Morris, 1993a, 2000). If previous reconstructions are indeed correct, then *Mackenzia* should possess some classic anemone

characteristics. Figure 13 also incorporates *Mackenzia* specimens that show similarities with our anemone experimental data. Figure 13-E and 13-D show long, dark bands running the length of the organism Such bands are markedly similar to the mesenteries of modern sea anemones, a feature not found in other organisms.

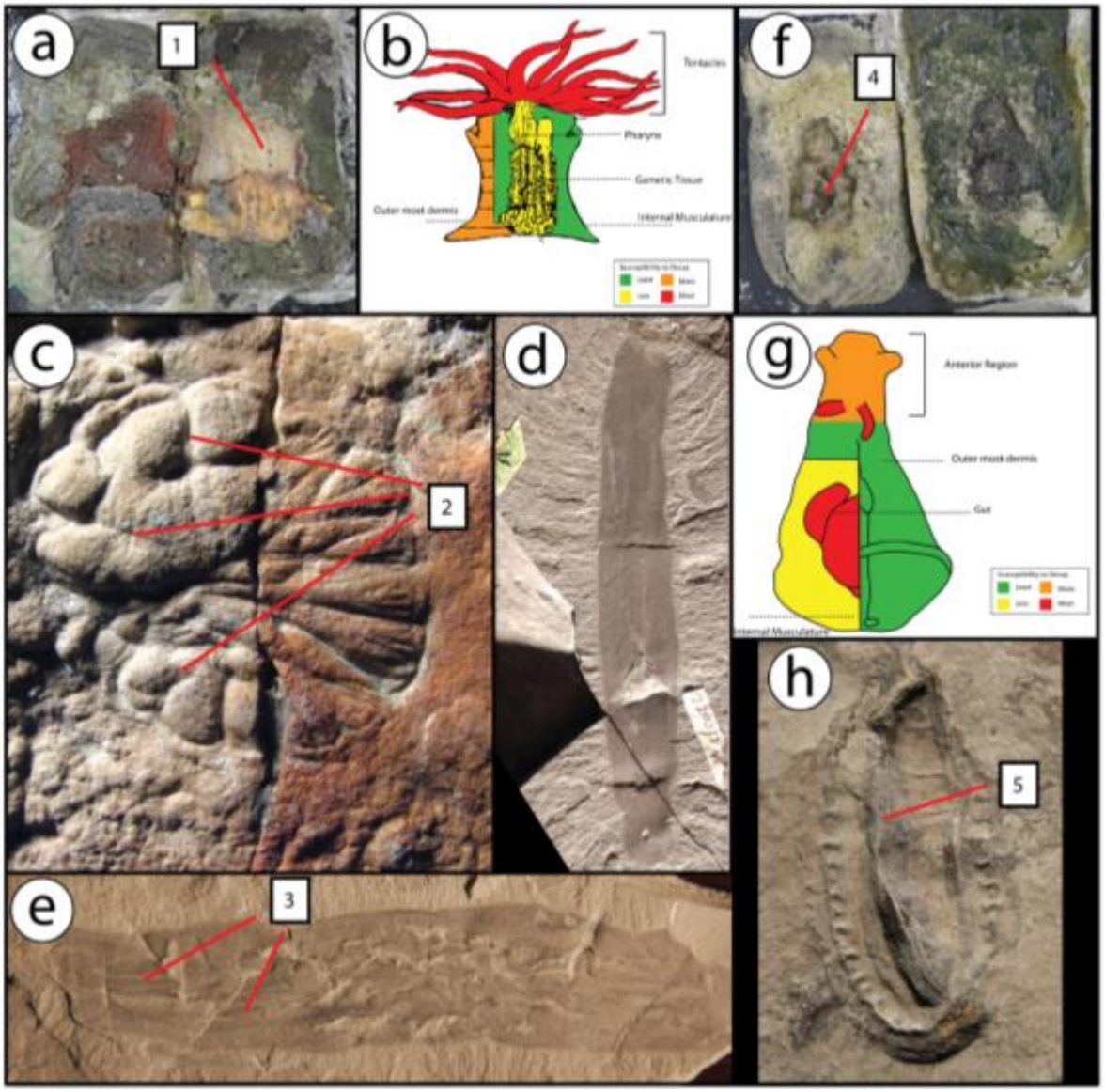

Figure 13. Fossil Comparisons for Cambrian and Ediacaran Fauna: Comparison of decay organisms from this study, and three Ediacaran or Cambrian fossils. (a) Sea anemone from Ediacaran-style decay experiment showing persistence off all anatomy, (b) decay index for anemone generated from this study, (c) Ediacaran fossil *Inaria* (specimen #) of South Australia, (d) Cambrian fossil *Mackenzia* (specimen #), (e) rotated view of *Mackenzia* showing interpreted mesenteries [3], (f) sea hare from Ediacaran-style decay experiment, showing cavity where carcass decayed from [4], (g) decay index for sea hares generated from this study, (h) *Kimberella* of White Sea Assemblage showing enhanced 3-D preservation (5).

The posterior portion of the organism has a very discrete bulbous end, which looks similar to holdfasts of the Ediacaran fronds, or the pedicle foot of anemones. Our assessment concurs with previous interpretations of *Mackenzia* as an anemone. Specimens of *Mackenzia* have not been collected with evidence of tentacles, but if such features were present they would likely have been lost in early decay, even under conditions favorable to soft-tissue preservation, as our decay experiments have demonstrated. We would also like to note the similarities with *Inaria*. Fossil *Inaria* are often garlic-shaped with dark, crevice-like structures running from the exterior of the fossil towards the center. These crevice-like structures appear similar to the mesenteries of anemones, similar to the dark bands noted on *Mackenzia*. Furthermore, *Inaria* fossils exhibit the same "folding over" pattern that our anemones did during the Ediacaran-style decay experiments. The thin anterior portion of *Inaria* often is observed to have folded over the bulbous bottom portion. This appears markedly similar to the body column of the anemones folding over their respective "foot".

Results from the triploblastic experiments also have implication for the fossil record, specifically interpreting Ediacaran fossils. The 'gut' of the sea hares in our decay experiments rapidly disappeared leaving just an outline of the carcasses in the form of the outer most dermal layer. The Ediacaran organism *Kimberella quadrata* (Glaessner & Wade, 1966) has been interpreted as a stem-group mollusk (Fedonkin, 2003; Fedonkin et al., 2007; Seilacher, 2007; Ivantsov 2009; Gehling et al., 2014), but this interpretation has also been challenged as well (Erwin, 1999). One of the strongest cautions against *Kimberella* as a mollusk is the lack of hemocoel, which all mollusks possess. According to Erwin (1999), if *Kimberella* were indeed a triploblastic organism, necessary for being a mollusk, it would have to have had this fluid-filled cavity. Given the results of our decay experiments, this key molluscan feature is lost rapidly within the taphonomic window, implying that *Kimberella*, unless preserving the entire internal structure, would most likely lose evidence of such a feature.

Lastly, in terms of the pyritic ‘death mask’ model for Ediacaran fossilization, our decay organisms did not produce the expected FeS precursors necessary for the classic Gehling (1999) ‘death mask’ model. Nor did the carcasses precipitate the expected element associations expected for a clay-centric ‘death mask’ model outlined in the Darroch et al. 2012 paper. One interpretation might be that there is a necessary dermal rigidity or complexity required for dense FeS precipitation to occur that was absent in the study organisms. Alternatively, the results presented may be taken as evidence that previously proposed models for Ediacaran preservation are inadequate, and potentially provide indirect support for the early silicification model recently proposed by Tarhan et al. (2017). Under this model, it is neither clay nor FeS that is driving enhanced soft-bodied preservation, but an increased flux of dissolved silica into the sediment surrounding freshly killed carcasses. Due to higher saturation in the ocean water from lack of silicate-biomineralizing organisms, silica is able to quickly diffuse into the subsurface sediment entombing the decaying organism early in the taphonomic window. Although this model is not directly refuted by the work presented here, more silica-inclusive tests need to be conducted to assess the likelihood of such a model.

CHAPTER 5

CONCLUSIONS

The results from our experiments illustrate that, although the overall pattern of decay is broadly similar in both baseline and Ediacaran-style experiments, the rate of decay in Ediacaran experiments are much slower overall, while also apparently accelerating the decay of certain phylogenetically important characters. In addition, slight differences in the patterns of decay between the two sets of experiments reveal that Ediacaran taphonomic scenarios potentially bias against the preservation of key diploblastic and triploblastic characters. Although outer dermal layers persist for long periods of time resulting in a clear outline of the organism, little in the way of internal or labile delicate external anatomy is likely to survive. This suggests that many enigmatic Ediacaran fossils could equally represent either diploblastic or triploblastic organisms, and that the taphonomic pathway may effectively prevent us from distinguishing between the two.

Our experiments also illustrate that the black 'decay halo' that precipitates outward from decaying carcasses in Ediacaran-style experiments does not correspond to either FeS or aluminosilicate precipitation. Although additional analyses should be conducted, we hypothesize that this enrichment of dark sand corresponds to increase organics dispersing from the carcass as it decays. Regardless, more work is required to better understand the direct relationship between the different interpretations of 'death mask' style preservation and this halo.

APPENDIX

Appendix 1: Elemental Percent Abundance Data

ID	time	C	O	Na	Mg	Al	Si	S	Cl	K	Ca	Ti	Fe
SA1A	0.5	23.22078422	46.27194024	1.122595495	0.969578274	0.355889865	22.99954174	0.463699761	4.252715295	0.07856964	0.152183206	0	0.112502269
SA1B	0.5	10.15884487	51.05094767	1.771456046	1.19962248	0.271572318	29.68153768	0.440878193	4.889858624	0.114150309	0.324391302	0	0.096740495
SA1C	0.5	19.68998345	47.90900418	2.67256718	0.488740764	0.870858453	24.51575739	0.334632885	3.095152084	0.049419809	0.124547664	0	0.249336148
SA2A	0.5	6.773514022	51.9665811	2.390239238	1.07276047	0.889633238	31.08869612	0.453713918	4.638647609	0.091523149	0.210320219	0	0.424370915
SA2B	0.5	8.228816901	50.62622266	3.073086016	1.048646713	1.218738411	29.96982947	0.353896302	4.802175109	0.05486533	0.213928672	0	0.409794406
SA2C	0.5	21.3351353	47.49737015	1.806596246	0.368922488	0.320459264	24.84093715	0.376977791	3.178297521	0.092789975	0.082565498	0	0.099948617
SA3A	0.5	13.11105995	49.76563511	2.497435861	1.023447697	0.317390327	28.08491741	0.335416355	4.318758477	0.094115492	0.119619318	0.264912712	0.06729129
SA3B	0.5	17.43527156	48.7887721	1.448458178	0.882852098	1.216458196	26.3034795	0.331558374	3.130562688	0.047441145	0.186779047	0	0.228367119
SA3C	0.5	20.64626394	47.54909008	2.14324084	0.380498136	1.688958381	23.51311103	0.307741729	3.204344263	0.052561819	0.107022706	0.168533391	0.238633693
SA4A	1	13.57453797	48.5448102	1.030914107	1.430694811	0.383037302	28.75977196	0.53982725	5.387457166	0.059230779	0.169017071	0	0.120701388
SA4B	1	24.49955497	46.66248698	1.51341935	0.593339701	1.119275057	22.43039797	0.243933022	2.3914431	0.06153011	0.06094588	0.131164006	0.29250986
SA4C	1	18.36432334	48.84694714	1.844415455	0.65228175	0.534625498	26.46713512	0.242568516	2.828082698	0.035865111	0.092923105	0	0.090832276
SA5A	1	19.79730889	44.97705542	1.856091402	2.637997643	0.326064579	21.21075203	0.822588337	7.816633886	0.197731916	0.23284748	0	0.124928426
SA5B	1	19.59977723	48.81369468	0.856184058	0.722701961	0.598933898	25.8158787	0.326937471	3.030641019	0.091373914	0.106409129	0	0.037467945
SA5C	1	15.41168001	49.86439863	1.705891445	0.628316759	0.472692501	28.22330083	0.253152703	3.147002223	0.089795045	0.129962431	0	0.073807424
SA6A	1	21.69118112	45.96376683	0.973803581	1.255227972	0.562116489	22.82074945	0.552185036	5.570538207	0.154756026	0.223528672	0	0.232146617
SA6B	1	20.62975547	48.24766258	1.016971742	0.843884674	0.698377433	24.29196818	0.32232786	3.168304133	0.058862464	0.103426237	0.278381693	0.340077532
SA6C	1	15.75655369	49.61190681	1.642027788	0.984118294	0.804505372	26.65932761	0.335734319	3.763855299	0.083050416	0.090257022	0	0.268663383
SA7A	2	16.53247471	47.39389505	1.767731967	1.226512014	0.945419626	25.6429206	0.452110866	5.614008175	0.122566225	0.144656977	0	0.157703796
SA7B	2	12.13289445	50.42291666	1.839383709	0.995672469	0.213258157	28.60939764	0.483750478	4.906565907	0.152876652	0.198403931	0	0.044879947
SA7C	2	11.42977564	51.04416008	1.950082586	0.769297859	0.314285957	29.79967829	0.379248105	4.030423191	0.090959148	0.095296878	0	0.096792271
SA8A	2	11.69532613	49.79061211	1.769650599	1.232065732	0.210986771	29.77316912	0.462114334	4.733452791	0.121217702	0.108628449	0	0.102776264
SA8B	2	6.175573125	52.53825933	1.499347084	0.906531034	0.255995805	33.81753172	0.308125166	4.211101047	0.105968316	0.082788538	0	0.098778829
SA9A	2	18.08243036	48.26885148	1.14450184	0.796355977	0.408006933	28.27515975	0.341814697	2.342006918	0.128207475	0.039833322	0	0.172831247

C

SA9AG	2	24.01686434	45.08009129	2.170973722	0.997020294	0.878837411	20.91260061	0.478125757	4.353980367	0.338637956	0.182198173	0.102166273	0.48850381
SA11A	8	17.44533664	47.74818999	2.1446656	1.178052344	0.968322865	25.38942512	0.091255942	4.287937962	0.094883687	0.251944862	0	0.399984984
SA11B	8	19.67610323	47.04243133	1.804896787	1.11939853	0.413326169	24.43151894	0.299250703	4.662672192	0.118209299	0.258234259	0	0.173958571
SA12A	8	18.21587442	48.32851192	1.972706691	0.864421692	0.57935927	26.07147105	0.252475818	3.250061065	0.084660916	0.149521349	0	0.230935807
SA12B	8	14.40297472	48.40620789	2.615902308	1.105024387	0.193534405	26.6427351	0.473405547	5.644060582	0.18947888	0.156617288	0	0.170058889
SA13A	13	9.169886461	51.40819404	1.61223206	1.50829758	0.831390319	29.49251488	0.08567051	5.433227953	0.098057362	0.141046193	0	0.219482649
SA13B	13	23.27890694	47.29309359	1.387821492	0.669990017	0.407007111	23.26217853	0.072777938	3.292439479	0.029892491	0.073781297	0	0.232111124
SA14A	13	11.80169195	50.33882343	1.563769191	0.959209325	0.246599562	29.59408944	0.078785395	5.044585581	0.080604571	0.116601957	0	0.175239599
SA14B	13	18.96353357	47.95233643	1.258675672	1.240712379	0.893319595	24.32779305	0.213997998	4.610702953	0.102898401	0.212989613	0	0.223040348
SA15A	13	14.74192692	48.94471494	1.281621668	1.389054687	0.39764343	28.80032742	0.192999096	3.838397747	0.059338184	0.097412307	0.108561667	0.148001931
SA15B	13	12.5291881	49.67912652	1.670659423	1.338017992	0.495943819	29.74125785	0.17974089	4.038397137	0.054313824	0.090549103	0	0.182805337
SA16A	27	22.9887302	46.18177654	1.527565566	0.759557933	0.656024327	23.91129281	0.081089059	3.551314444	0.053721035	0.13266971	0	0.156258363
SA16B	27	20.96456088	47.08179193	1.48069835	0.968480931	0.374292832	24.7521512	0.068762546	4.031589193	0.055051595	0.10712997	0	0.115490572
SA17A	27	29.50265013	42.80866393	1.786517362	1.005760374	0.218245592	19.39345976	0.097932645	4.63005612	0.111673236	0.210765025	0.126821862	0.107453955
SA17B	27	30.44149466	44.63640534	1.014803866	0.5128634	0.308135941	19.80675275	0.039991973	3.004787084	0.036388001	0.083522676	0	0.114854309
SA18A	27	25.2433242	46.02226588	1.412750011	0.926646253	0.386635334	22.13969541	0.144465368	3.538892126	0.039840666	0.077897339	0	0.067587406
SA18B	27	22.95760394	46.76477211	1.198713713	0.897329497	0.220462949	23.65100984	0.174980601	3.823075915	0.040246905	0.137132364	0	0.134672179
SA19A	34	23.51332458	46.92876108	1.685380553	0.716339753	0.231805587	23.00987495	0.15918802	3.40366811	0.067166202	0.096178261	0	0.188312908
SA19B	34	24.80086359	46.36109831	1.696892041	0.711191258	0.400509851	22.33357872	0.055098884	3.2684408	0.07999659	0.177903149	0	0.1144268
SA20A	34	27.67807829	43.62677287	1.432157809	1.111423966	0.321699354	21.45098492	0.243198403	3.707399677	0.146394447	0.137483764	0	0.1444065
SA20B	34	21.74446072	46.23128184	1.564480467	1.160226969	0.146621906	24.301511	0.215111722	4.297508214	0.103765409	0.097415017	0	0.137616737
SA21A	34	23.31596221	46.65676032	1.459884736	0.917793128	0.843653222	22.42848673	0.097432434	3.745721655	0.132235757	0.060916991	0	0.341152823
SA21B	34	17.02520816	48.23858235	1.485468458	0.754431123	0.210341526	28.08149611	0.056710279	3.861230034	0.096393389	0.096832475	0	0.093306104
SA22A	41	33.24000869	43.13836244	1.160766709	0.499477775	0.42965514	18.27988734	0.047406826	3.097993911	0.043217965	0.011712882	0	0.051510326
SA22B	41	22.3444397	48.35640093	1.056543588	0.658096607	0.20990203	23.95323503	0.514793909	2.703355902	0.051947672	0.077403749	0	0.073880886
SA23A	41	18.9017684	48.04473786	1.121820402	0.882131274	0.516645258	26.19955047	0.073565135	3.906467401	0.09205161	0.120286487	0	0.140975696
SA23B	41	24.59522133	46.70051702	1.12282347	0.586950324	0.719608748	23.20527648	0.069805558	2.791488495	0.044308085	0.055886936	0	0.108113551

C

SA24A	41	20.32479313	47.58306862	1.375246167	0.810697165	0.258507163	25.1558932	0.206041636	4.03110583	0.052885319	0.089050277	0	0.112711499
SA24B	41	11.88083068	50.61075083	1.167753454	0.824657838	0.256658481	30.66623983	0.357923784	3.983199264	0.047644777	0.105509222	0	0.098831843
SA25A	56	20.53087356	46.85020098	1.221024788	0.950579878	0.511492045	25.25064345	0.129363612	4.203992387	0.09346765	0.024596072	0	0.233765573
SA25B	56	23.46380551	47.29209018	1.025798735	0.676355163	0.361518978	24.47393791	0.043015819	2.408428759	0.010736174	0.014844539	0.1329065	0.096561738
SA26A	56	20.9511382	45.90503577	1.849911121	0.949173343	0.20644728	24.23669077	0.099197778	5.515170981	0.103770549	0.086854716	0	0.096609495
SA26B	56	25.38373951	45.51800629	1.694111348	1.090140515	0.771396954	20.57145226	0.09517091	4.399373246	0.05794936	0.104762194	0	0.313897414
SA27A	56	30.49343973	41.23654361	1.556872434	1.685655211	0.543515905	18.21725204	0.17565223	5.25697053	0.127973692	0.449802487	0	0.256322131
SA27AA	56	21.71900994	45.53381659	1.899001464	1.493526779	0.638473395	22.85927595	0.103668277	5.170987923	0.170330065	0.289373908	0	0.122535713
SA27B	56	22.99701868	46.77067238	1.323978367	1.192923835	0.735377817	21.67691526	0.072076072	4.645169059	0.122593219	0.095028425	0.07345469	0.294792189
SA28A	68	24.23692489	44.00970851	2.015978734	1.146452275	0.358747325	23.05101397	0.194458237	4.490938174	0.115956917	0.215933382	0	0.163887579
SA28B	68	25.50925678	45.32264208	1.200790833	0.779241892	0.273883573	22.49598334	0.145558829	3.956921934	0.11412864	0.101723229	0	0.099868875
SA29A	68	21.73053229	46.4753628	1.819526369	1.093815497	0.284800174	23.44484075	0.062692759	4.815350091	0.120966547	0.019030242	0	0.133082473
SA29B	68	25.18322859	45.94534355	1.386952046	0.975963584	0.654688861	22.63743121	0.047248174	2.840098679	0.076016098	0.024621272	0	0.228407937
SA30A	68	24.2582722	44.4409194	1.924734394	1.122192978	0.590442998	22.84894588	0.191221074	4.24508078	0.101773316	0.106215677	0	0.170201306
SA30B	68	25.47785359	47.26281455	1.13866364	0.552307887	0.365477522	22.98445945	0.058241867	2.047688337	0.031680443	0.028811305	0	0.052001422
SA31A	79	26.36577586	45.74798251	1.756534322	0.359965852	0.313405666	22.18226854	0.155393517	2.891749209	0.032904849	0.065071263	0	0.128948401
SA31B	79	18.61197595	47.84761046	2.289156494	0.68875695	0.217174716	25.74293493	0.204079469	4.01410195	0.087312489	0.223883352	0	0.073013244
SA31C	79	20.95701976	48.14495847	2.145730479	0.615138329	0.713645406	24.33849717	0.158667376	2.66831983	0.073046539	0.083864074	0	0.101112565
SA32A	79	19.74361811	46.61908322	1.553928154	1.015276252	0.177824614	24.97860103	0.180273785	5.381818317	0.128292977	0.077909114	0	0.143374427
SA32B	79	21.888401	47.8866891	1.100118238	0.619151513	0.469770504	24.95173759	0.076566046	2.828396578	0.062289096	0.032793746	0	0.084086589
SA33A	79	15.0454912	48.95303421	1.615795978	1.020506855	1.270713198	26.74739745	0.080913688	4.736382326	0.115362896	0.05226982	0	0.362132374
SA33B	79	11.22909652	50.68288652	1.556174803	1.013823262	0.452923426	30.19645372	0.085955956	4.406163361	0.153147203	0.044124353	0	0.179250872
N1A	0.5	11.91442887	50.88814742	1.425123619	1.032587871	0.43160787	28.66324275	0.370152009	4.991305234	0.095124614	0.188279745	0	0
N1B	0.5	13.45812073	50.39241057	1.195399774	1.109922585	0.341628752	27.96217508	0.51129574	4.709810035	0.097864698	0.221372034	0	0
N1C	0.5	10.21676766	51.51004107	1.359676219	0.851349693	0.250970313	31.43681576	0.350519033	3.659812836	0.085783681	0.150064657	0	0.128199085
N2A	0.5	13.17701772	48.69033143	2.854877695	1.189906013	0.416045356	27.00083956	0.466723222	5.714498509	0.071632241	0.222129654	0	0.195998607
N2B	0.5	7.857667619	51.99156633	1.903302407	0.805431191	0.575141188	32.30475621	0.390681276	3.771366203	0.089736227	0.135255291	0	0.175096056

C

N2C	0.5	11.04140015	50.35073365	2.784070695	0.717301477	0.624158733	29.48598527	0.332229198	4.159132717	0.061993642	0.115090369	0	0.327904103
N3A	0.5	5.612274739	51.35986271	1.715165711	1.772903396	1.069815601	30.96691909	0.429325137	6.201429361	0.104164158	0.22074604	0	0.547394055
N3B	0.5	13.49994746	49.86435844	1.783359531	1.040041676	0.867227007	28.54107525	0.288253136	3.583210067	0.059605203	0.116891497	0.138895839	0.217134892
N3C	0.5	18.60086667	48.12312964	2.975055544	0	0.427889451	26.19435765	0.277401184	3.143316398	0.10173449	0.102359868	0	0.053889107
N4A	1	5.623002327	51.74834048	1.6925276	1.345457951	0.883658661	32.57803859	0.478430053	5.137893961	0.115862853	0.217610473	0	0.179177058
N4B	1	21.01809893	47.48642005	1.955874357	0.502440119	0.907488212	24.86928064	0.231430329	2.53218958	0.057588843	0.109337706	0.080829612	0.249021619
N4C	1	19.00177309	47.14102173	2.355520111	0.819413298	0.870700928	25.40630003	0.365988936	3.506082399	0.090739111	0.134235616	0	0.30822476
N5A	1	11.94962687	49.17936124	1.741967806	1.414812528	0.627266613	28.3396135	0.540413863	5.493505026	0.118016216	0.264427915	0	0.330988424
N5B	1	13.3956517	50.06493057	1.532489115	0.875379873	0.607065362	29.35201039	0.352054936	3.442428005	0.092067572	0.161966349	0	0.123956131
N5C	1	15.94966767	49.51436716	1.421067782	0.748988654	0.765374409	28.12205358	0.270201097	2.770417477	0.04585415	0.09768112	0	0.294326898
N6A	1	17.10577903	48.66825837	1.595331669	0.543414551	0.3876907	27.31237075	0.303213942	3.693798329	0.083419922	0.111976925	0	0.194745805
N7A	2	18.98380555	48.26787383	2.087629549	0.440398415	0.567766279	26.01074866	0.29991191	3.005869172	0.077295179	0.093034437	0	0.165667027
N7B	2	29.74558361	43.54072922	1.365407742	0.887484171	0.349489931	19.50973584	0.372546406	3.740160237	0.152171026	0.22576467	0	0.110927144
N7C	2	14.09885235	50.86955927	1.570738117	0.753229742	1.32733182	27.3171736	0.26821015	3.061972187	0.070859008	0.118703745	0	0.543370017
N8A	2	12.84961866	50.8765081	1.892783186	0.738897476	0.884089263	29.42762759	0.23608419	2.764865694	0.081720122	0.14553972	0	0.102265991
N8B	2	17.81708232	47.44450177	2.503437915	0.902185409	0.836659816	25.21030109	0.300188096	4.286579529	0.074162054	0.474930876	0	0.149971124
N8C	2	13.91386737	48.25530878	2.56568502	1.105644156	0.495002692	26.91918195	0.496442492	5.463972543	0.184990212	0.379999947	0	0.219904839
N9A	2	14.82512008	48.74136881	2.123994301	0.949960018	0.782507106	27.44308579	0.281625992	3.877277331	0.068367319	0.286718412	0.316872181	0.303102669
N9B	2	15.05841294	48.20018463	2.301821017	0.906737962	0.468734812	27.84108552	0.385420641	4.156330943	0.094159302	0.381400153	0	0.205712086
N10A	8	19.49601406	46.53906899	1.775581461	1.498778144	0.304353893	22.3994362	0.388503366	6.364904116	0.168726344	0.735527809	0.158839849	0.17026578
N10B	8	16.99744021	48.37929609	1.520140703	0.804681464	0.765554318	25.78448694	0.357908933	4.558330729	0.093547278	0.42497521	0	0.313638116
N11A	8	11.99318407	51.24881846	1.806363442	0.521568054	0.899722762	30.34709673	0.177496593	2.590498019	0.045024219	0.150138596	0	0.220089062
N11B	8	13.23787394	50.30271278	1.364856354	0.709706348	0.355652655	29.82522659	0.244952604	3.53202572	0.072060567	0.131203764	0	0.223728686
N12A	8	22.46975899	44.80416273	2.510827285	0.971248257	1.298969944	22.79311011	0.188403796	4.115115508	0.082438036	0.453301177	0	0.312664159
N12B	8	15.88191679	47.11796319	2.437557477	1.014307903	0.653637466	25.40075486	0.387216548	6.372762133	0.106305252	0.443132682	0	0.184445697
N13A	13	17.61904384	47.07402917	2.010563025	1.079039861	0.568666536	25.79392556	0.069995646	4.968422925	0.145853644	0.561754266	0	0.108705535
N13B	13	18.86955724	46.40949546	2.153527158	1.143467706	0.552888767	25.01596223	0.091258055	5.071682366	0.074872188	0.37438484	0	0.242903997

C

N14A	13	14.18240886	47.40489405	2.254851037	1.14976943	0.365077445	28.03599888	0.086925048	5.591384031	0.083036793	0.467054665	0.232927218	0.145672541
N14B	13	23.59497534	47.29332369	1.21609652	0.667619313	1.087357946	22.45740826	0.187942086	2.83271465	0.074181217	0.230134604	0	0.358246376
N15A	13	16.29291831	48.40692818	1.639429677	0.926758062	0.269374283	26.97653906	0.207616113	4.717684755	0.096888487	0.366951291	0	0.098911785
N15B	13	11.44190148	50.30243592	1.698608731	1.0233287	0.577276336	30.09593445	0.164146046	4.239368453	0.082996096	0.227279504	0	0.14672428
N16A	27	21.81904572	46.26663451	1.632956159	1.061671134	0.128314058	23.23721723	0.204566489	4.810722861	0.202653003	0.529037195	0	0.10718165
N16B	27	16.25571767	49.23486771	2.109942651	0.777478041	0.938741263	26.76418585	0.071413893	3.355236332	0.060185058	0.190971815	0	0.241259716
N17A	27	20.55142569	46.61146142	1.667818862	1.434747639	0.82872774	22.89436136	0.153010606	5.143553691	0.09263398	0.36064659	0	0.261612419
N17B	27	16.65557627	48.80452768	2.019495343	0.733066196	0.379836686	27.06600033	0.228629789	3.820025787	0.078540601	0.154365959	0	0.059935353
N18A	27	20.29916144	46.10599157	1.638414866	0.978478451	0.968624052	24.25767064	0.205054912	4.291247123	0.135660557	0.752887799	0	0.3668086
N18B	27	13.55457288	49.79053299	1.450424357	0.8689449	0.244211244	29.37243678	0.156649676	3.860163321	0.119622458	0.476951282	0	0.105490111
N19A	34	21.57471445	46.66986234	1.736702364	1.067062777	0.415872669	23.24639958	0.186826605	4.152384558	0.128092212	0.539804046	0	0.282278403
N19B	34	17.1679678	48.22993069	1.553164351	0.924820714	0.358832329	26.61966988	0.11938937	4.40057364	0.098625454	0.393721022	0	0.133304749
N20A	34	14.74678373	49.01452241	1.888302184	1.145909194	0.167226843	27.28460469	0.173384737	4.695827375	0.144265215	0.61194609	0	0.127227535
N20B	34	18.1538685	46.76845612	2.470176688	0.938660538	0.407359708	25.95619771	0.112536414	4.421789768	0.093519699	0.498438506	0	0.178996351
N21A	34	15.74893324	47.35126692	2.357645159	1.05397005	0.43637688	25.91914103	0.110690763	6.233228985	0.110032389	0.443667604	0	0.235046986
N21B	34	20.90620938	46.24597667	2.051379364	0.869284047	1.30052531	23.95685458	0.039150222	3.734173698	0.069610724	0.284165958	0.072157361	0.470512678
N22A	41	26.2918051	44.68475205	1.750000714	0.989676422	0.4569855	20.4057617	0.144600904	4.410931657	0.099442408	0.527242861	0	0.238800678
N22B	41	14.18413937	49.38558133	2.026963508	1.122929699	0.361574125	27.68272437	0.110185543	4.47470474	0.116381025	0.423182674	0	0.111633616
N23A	41	23.43397146	45.41753201	1.811337191	0.718737047	0.209072545	22.97907446	0.10525144	4.602986949	0.084799679	0.291233557	0.243182571	0.10282109
N23B	41	18.8710932	48.15722603	1.429354151	0.79481578	0.548034235	27.31239407	0.035347927	2.264049452	0.061204672	0.221175234	0.086793837	0.218511398
N24A	41	21.53852017	45.72567072	2.201642024	1.06552629	0.444315106	23.93149867	0.167900525	4.251566551	0.113216914	0.480676554	0	0.079466479
N24B	41	21.51727955	46.52489606	1.662520065	0.770414044	0.806171422	23.97762936	0.079645227	3.54257521	0.077662955	0.348722006	0.326452598	0.36603151
N25A	56	19.77515942	47.43180644	2.22316987	0.771360097	0.553123092	24.5975372	0.364306027	3.84637445	0.055588994	0.065334649	0.072719567	0.243520193
N25B	56	24.90148828	45.56461099	1.844738419	0.804154287	0.246449884	22.12126023	0.368296708	3.929335213	0.081214886	0.065918843	0	0.07253225
N26A	56	17.43233662	45.87148062	2.74226629	1.476317584	0.502127286	24.12698287	0.514792734	6.987233895	0.15053185	0.076724424	0	0.119205823
N26B	56	25.12880318	45.27765347	1.327922979	0.833560551	0.377345417	22.02108192	0.471702896	4.116525837	0.148185809	0.11851902	0	0.178698926
N26C	56	17.57202475	48.4661968	1.879099278	0.79320059	0.481945152	25.93913378	0.469602358	3.929979748	0.119233872	0.157777803	0	0.19180588

C

N27A	56	29.81482429	42.74619318	2.231971588	0.846342218	0.347266924	19.4581741	0.184162732	3.93169923	0.101657188	0.230931465	0	0.106777092
N27B	56	14.05146261	50.38537458	1.809816582	0.497501024	1.107499953	29.39862525	0.043870705	2.476672981	0.059873574	0.077021621	0	0.092281127
N28A	68	26.86368124	42.2952499	2.642165276	1.470005807	0.227553681	19.97303261	0.270224103	5.578919535	0.245330242	0.344743561	0	0.089094056
N28B	68	26.1270899	44.8061766	1.589272763	0.770029014	0.534871936	21.6445491	0.085752154	4.106045909	0.05469447	0.102303361	0	0.179214789
N29A	68	21.94983534	46.81244941	1.852431566	0.61767982	0.190782407	23.90547779	0.356517732	3.930899735	0.111405136	0.132179434	0	0.140341632
N29B	68	22.25040003	47.01089937	1.459585826	0.474357563	0.310658652	24.21234334	0.47068991	3.276241831	0.103533436	0.084799967	0.197414675	0.1490754
N29C	68	15.24062213	50.61276997	1.281651869	0.381390853	0.382840598	29.68051317	0.351200183	1.819262975	0.068460755	0.072764192	0	0.108523314
N30A	68	25.90086342	45.06276806	1.932773661	0.840021687	0.30680035	21.84946087	0.147076749	3.571607081	0.125525162	0.157069668	0	0.106033292
N30B	68	22.61840111	46.7657007	1.878342027	0.843853518	1.377384654	22.23763309	0.087247009	3.521612331	0.076415751	0.114401815	0	0.479008
N31A	79	29.91618954	42.65588661	2.239062379	0.993299115	0.821427299	17.731097	0.242857048	4.649836939	0.097662626	0.389300581	0	0.263380863
N31B	79	20.89545093	47.43673534	1.872355228	0.631654208	1.026220285	24.16011329	0.06532109	3.52479604	0.073188677	0.106723325	0	0.207441599
N32A	79	17.74222833	49.53040673	1.445293326	0.4087413	0.508424769	26.71408217	0.318613466	2.943479096	0.056701971	0.16262953	0	0.169399305
N32B	79	21.34160882	47.35015547	2.021916587	0.580831132	2.250993573	22.68065454	0.277794362	2.808897795	0.04587544	0.118839197	0	0.522433086
N33A	79	20.24197633	45.38090446	2.573030582	1.168686068	0.468888627	23.74592844	0.232773804	5.554208391	0.148348179	0.281982485	0	0.203272627
N33B	79	17.89773037	48.4172558	1.781399035	0.758397611	0.520458943	26.81743195	0.145176353	3.236152695	0.053982507	0.193285198	0	0.178729531

REFERENCES

ANDERSON, E.P., SCHIFFBAUER, J.D., AND XIA, S., 2011, Taphonomic study of Ediacaran organic-walled fossils confirms the importance of clay minerals and pyrite in Burgess Shale-type preservation: Geology, v. 39, p. 643–646, doi: 10.1130/G31969.1.

BRIGGS, D.E.G., 2003, The role of decay and mineralization in the preservation of soft-bodied fossils: Annual Review of Earth and Planetary Sciences, v. 31, p. 275–301, doi: 10.1146/annurev.earth.31.100901.144746.

BRIGGS, D.E.G. AND MCMAHON, S., 2016, The role of experiments in investigating the taphonomy of exceptional preservation: Palaeontology, v. 59, p. 1–11, doi: 10.1111/pala.12219.

BRUSCA, R.C., 1980, Common Intertidal Invertebrates of the Gulf of California: University of Arizona Press.

BUDD, G.E. AND JENSEN, S., 2000, A critical reappraisal of the fossil record of the bilaterian phyla: Biological Reviews, v. 75, p. 253-295.

BUSS, L.W. AND SEILACHER, A., 1994, the Phylum Vendobionta - a Sister Group of the Eumetazoa: Paleobiology, v. 20, p. 1–4, doi: 10.2307/2401145.

BUTTERFIELD, N.J., 1995, Secular distribution of Burgess Shale-type perservation: Lethaia, v. 28, p. 1-3, doi:?.

CALLOW, R.H.T. AND BRAISER, M.D., 2009, Remarkable preservation of microbial mats in Neoproterozoic siliciclastic settings: Implications for Ediacaran taphonomic models: Earth-Science Reviews, v. 96, p. 207–219, doi: 10.1016/j.earscirev.2009.07.002.

CAMERON, C.B., 2002, Particle retention and flow in the pharynx of the enteropneust worm *Harrimania planktophilus*: The filter-feeding pharynx may have evolved before the chordates: Biological Bulletin, v. 202, p. 192–200.

CASENOVE, D., OJI, T., AND GOTO, T., 2011, Experimental Taphonomy of Benthic Chaetognaths:

C

Implications for the Decay Process of Paleozoic Chaetognath Fossils: Paleontological Research, v. 15, p. 146–153, doi: 10.2517/1342-8144-15.3.146.

CONWAY MORRIS, S., 1989, Burgess shale faunas and the Cambrian Explosion: Science, v. 246, p. 339–346, doi: 10.1126/science.246.4928.339.

CONWAY MORRIS, S., 1993a, Ediacaran-like fossils in Cambrian Burgess shale-type faunas of North America: Palaentology, v. 36, p. 593–635.

CONWAY MORRIS, S., 1993b, The fossil record and the early evolution of the Metazoa: Nature, v. 361, p. 219–225, doi: 10.1038/361219a0.

CONWAY MORRIS, S., 2000, The Cambrian "explosion": slow-fuse or megatonnage? Proceedings of the National Academy of Sciences of the United States of America, v. 97, p. 4426–4429, doi: 10.1073/pnas.97.9.4426.

CUI, H., KAUFMAN, A.J., XIAO, S., PEEK, S., CAO, H., MIN, X., CAI, Y., SIEGEL, Z., LIU, X., PENG, Y., SCHIFFBAUER, J.D., AND MARTIN, A.J., 2016, Environmental context for the terminal Ediacaran biomineralization of animals: Geobiology, v. 14, p. 344–363, doi: 10.1111/gbi.12178.

DARROCH, S.A.F., LAFLAMME, M., SCHIFFBAUERJ. D., AND BRIGGS, D.E.G., 2012, Experimental Formation of a Microbial Death Mask: PALAIOS, v. 27, p. 293–303, doi: 10.2110/palo.2011.p11-059r.

DARROCH, S.A.F., SPERLING, E.A., BOAG, T.H., RACICOT, R.A., MASON, S.J., MORGAN, A.S., TWEEDT, S., MYROW, P., JOHNSTON, D.T., ERWIN, D.H., AND LAFLAMME, M., 2015, Biotic replacement and mass extinction of the Ediacara biota: Proceedings of the Royal Society B, v. 282.

DROSER, M.L. AND GELING, J.G., 2008, Synchronous aggregate growth in an abundant new Ediacaran tubular organism: Science, v. 319, p. 1660-1662.

DROSER, M.L., GEHLING, J.G., AND JENSEN, S.R., 2006, Assemblage palaeoecology of the Ediacara biota: The unabridged edition? Palaeogeography, Palaeoclimatology,

C

Palaeoecology, v. 232, p. 131–147, doi: 10.1016/j.palaeo.2005.12.015.

ERWIN, D.H., 1999, The origin of bodyplans: American Zoologist, v. 39, p. 617-629.

ERWIN, D.H., LAFLAMME, M., TWEEDT, S.M., SPERLING, E. A., PISANI, D., AND PETERSON, K.J., 2011, The Cambrian Conundrum: Early Divergence and Later Ecological Success in the Early History of Animals: Science, v. 334, p. 1091–1097, doi: 10.1126/science.1206375.

FEDONKIN, M.A. AND WAGGONER, B.M., 1997, The Late Precambrian fossil *Kimberella* is a mollusc-like bilaterian organism: Nature, v. 388, p. 868–871, doi: 10.1038/42242.

FEDONKIN, M.A., 2003, The origin of the Metazoa in the light of the Proterozoic fossil record: Paleontological Research, v. 7, p. 9-41.

FERRIS, F.G., SCHULTZE, S., WITTEN, T.C., FYFE W.S., AND BEVERIDGE, T.J., 1989, Metal interactions with microbial biofilms in acidic and neutral pH environments: Applied and Environmental Microbiology, v. 55, p. 1249-1257.

GEHLING, J.G., 1988, A cnidarian of actinian-grade from the Ediacaran Pound Subgroup, South Australia: An Australasian Journal of Palaeontology, v. 12, p. 299–314, doi: 10.1080/03115518808619129.

GEHLING, J.G., 1991, The case of Ediacaran fossil roots to the metazoan tree: Memoirs - Geological Society of India, v. 20, p. 181–224.

GEHLING, J.G., 1999, Microbial mats in terminal Proterozoic siliciclastics; Ediacaran death masks: PALAIOS, v. 14, p. 40–57, doi: 10.2307/3515360.

GEHLING, J.G., DROSER, M.L., JENSEN, S.R., AND RUNNEGAR, B.N., 2005, Ediacara Organisms: Relating Form to Function, in Briggs, D.E.G., ed., Evolving Form and Function: Fossils and Development, Proceedings of a Symposium Honoring Adolf Seilacher for His Contributions to Paleontology in Celebration of His 80th Birthday: Peabody Museum of Natural History, New Haven, Connecticut, p. 43–66.

GEHLING, J.G., RUNNEGAR, B.N., AND DROSER, M.L., 2014, Scratch traces of large Ediacara bilaterian animals: Journal of Paleontology, v. 88, p. 284-298, doi: 10.1666/13-054.

C

GLAESSNER, M.F. AND WADE, M., 1966, The late Precambrian fossils from Ediacara, South Australia: Palaeontology, v. 9, p. 599–628.

IVANTSOV, A.Y., 2009, New reconstruction of *Kimberella*, problematic Vendian metazoan: Paleontological Journal, v. 43, p.601-611, doi: 10.1134/S003103010906001X.

LAFLAMME, M., SCHIFFBAUER, J.D., NARBONNE, G.M., AND BRIGGS, D.E.G., 2010, Microbial biofilms and the preservation of the Ediacara biota: Lethaia, doi: 10.1111/j.1502-3931.2010.00235.x.

LEARY, S., UNDERWOOD, W., ANTHONY, R., AND CARTNER, S., 2013, AVMA Guidelines for the Euthanasia of Animals: 2013 Edition: 98 p.

LIU, A.G., KENCHINGTON, C.G., AND MITCHELL, E.G., 2015, Remarkable insights into the paleoecology of the Avalonian Ediacaran macrobiota: Gondwana Research, v. 27, p. 1355–1380, doi: 10.1016/j.gr.2014.11.002.

LIU, A.G., MATTHEWS, J.J., AND MCILROY, D., 2016, The Beothukis/Culmofrons problem and its bearing on Ediacaran macrofossil taxonomy: Evidence from an exceptional new fossil locality: Palaeontology, v. 59, p. 45–58, doi: 10.1111/pala.12206.

MAPSTONE, N.B. AND MCILROY, D., 2006, Ediacaran fossil preservation: Taphonomy and diagenesis of a discoid biota from the Amadeus Basin, central Australia: Precambrian Research, v. 149, p. 126–148, doi: 10.1016/j.precamres.2006.05.007.

MCMAHON, S., TARHAN, L.D., AND BRIGGS. D.E.G., 2017, Decay of the sea anemone *Metridium* (Actiniaria): implications for the preservation of cnidarian polyps and other soft-bodied diploblast-grade animals: Palaios, v. 32, p.388-395, doi: 10.2110/palo.2016.102.

MEYER, M., ELLIOTT, D., SCHIFFBAUER, J.D., HALL, M., HOFFMAN, K.H., SCHNEIDER, G., VICKERS-RICH, P., AND XIAO, S., 2014, Taphonomy of the Ediacaran Fossil *Pteridinium* Simplex Preserved Three-Dimensionally in Mass Flow Deposits, Nama Group, Namibia: Journal of Paleontology, v. 88, p. 240–252, doi: 10.1666/13-047.

MEYER, M., ELLIOTT, D., WOOD, A.D., POLYS, N.F., COLBERT, M., MAISANO, J.A.,

C

VICKERS=RICH, P., HALL, M., HOFFMAN, K.H., SCHNEIDER, G., AND XIAO, S., 2014, Three-dimensional microCT analysis of the Ediacara fossil *Pteridinium* simplex sheds new light on its ecology and phylogenetic affinity: Precambrian Research, v. 249, p. 79-87, doi: 10.1016/j.precamres.2014.04.013.

MEYER, M., SCHIFFBAUER, J.D., XIAO, S., CAI, Y., AND HUA, H., 2012, Taphonomy of the Upper Ediacaran Enigmatic Ribbonlike Fossil *Shaanxilithes*: Palaios, v. 27, p. 354–372, doi: 10.2110/palo.2011.p11-098r.

NANGLU, K., CARON, J.-B., AND CAMERON, C.B., 2015, Using experimental decay of modern forms to reconstruct the early evolution and morphology of fossil enteropneusts: Paleobiology, v. 41, p. 460–478, doi: 10.1017/pab.2015.11.

NARBONNE, G.M., 2005, The Ediacara Biota: Neoproterozoic Origin of Animals and Their Ecosystems: Annual Review of Earth and Planetary Sciences, v. 33, p. 421–442, doi: 10.1146/annurev.earth.33.092203.122519.

NATION, J.L., 1983, A new method using hexamethyldisilazane for preparation of soft insect tissues for scanning electron microscopy.: Stain technology, v. 58, p. 347–51, doi: 10.3109/10520298309066811.

NOFFKE, N., 2013, Geobiology: Microbial Mats in Sandy Deposits from the Archean Era to Today: 1689-1699 p.

NOFFKE, N., Knoll, A.H., AND GROTZINGER, J.P., 2002, Sedimentary Controls on the Formation and Preservation of Microbial Mats in Siliciclastic Deposits: A Case Study from the Upper Neoproterozoic Nama Group, Namibia: PALAIOS, v. 17, p. 533–544.

NORRIS, R.D., 1989, Cnidarian taphonomy and affinities of the Ediacara biota: Letahaia, v. 22, p. 381–393, doi: 10.1111/j.1502-3931.1989.tb01439.x.

ORR, P.J., BRIGGS, D.E.K., AND KEARNS, S.L., 1998, Cambrian Burgess Shale animals replicated in clay minerals: Science, v. 281, p. 1173-1175, doi: 10.1126/science.281.5380.1173.

C

PARK, E., HWANG, D.S., LEE, J.S., SONG, J.I., SEO, T.K., AND WON, Y.J., 2012, Estimation of divergence times in cnidarian evolution based on mitochondrial protein-coding genes and the fossil record: Molecular Phylogenetics and Evolution, v. 62, p. 329–345, doi: 10.1016/j.ympev.2011.10.008.

PEK, I., VAŠÍČEK, Z., ROČEK, Z., HAJN, V., AND MIKULÁŠ, R., 1996, Základy zoopaleontologie: Vydavatelství Univerzity Palackého, Olomouc, 264 p.

PETERSON, K.J., WAGONNER, B., AND HAGADORN, J.W., 2003, A fungal analog for Newfoundland Ediacaran fossils? Integrative and Comparative Biology, v. 43, p. 127–36, doi: 10.1093/icb/43.1.127.

RETALLACK, G.J., 1994, Were the Ediacaran fossils lichens? Paleobiology, v. 20, p. 523–544.

SANSOM, R.S., GABBOTT, S.E., AND PURNELL, M. a, 2011, Decay of vertebrate characters in hagfish and lamprey (Cyclostomata) and the implications for the vertebrate fossil record.: Proceedings. Biological sciences / The Royal Society, v. 278, p. 1150–1157, doi: 10.1098/rspb.2010.1641.

SANSON, R.S., GABBOTT, S.E., AND PURNELL, M. a, 2010, Non-random decay of chordate characters causes bias in fossil interpretation.: Nature, v. 463, p. 797–800, doi: 10.1038/nature08745.

SCHIFFBAUER, J.D., XIAO, S., CAI, Y., WALLACE, A.F., HUA, H., HUNTER, J., XU, H., PENG, Y., AND KAUFMAN, A.J., 2014, A unifying model for Neoproterozoic-Palaeozoic exceptional fossil preservation through pyritization and carbonaceous compression.: Nature communications, v. 5, p. 5754, doi: 10.1038/ncomms6754.

SEILACHER, A., 1989, Vendozoa: Organismic construction in the Proterozoic biospehere: Lethaia, v. 22, p. 229–239.

SEILACHER, A., 1999, Biomat-related lifestyles in the Precambrian: PALAIOS, v. 14, p. 86–93, doi: 10.2307/3515363.

SEILACHER, A., 2007, Trace Fossil Analysis: Springer Verlag, Berlin Heidelberg New York.

C

SEILACHER, A., GRAZHDANKIN, D., AND LEGOUTA, A., 2003, Ediacaran biota: The dawn of animal life in the shadow of giant protists: Paleontological Research, v. 7, p. 43–54, doi: 10.2517/prpsj.7.43.

SEILACHER, A. AND F. PFLÜGER, 1994, From biomats to benthic agriculture: a biohistoric revolution: Biostabilization of sediments, p. 97-105.

SOKOLOV, B.S. AND FEDONKIN, M.A., 1984, The Vendian as the Terminal System of the Precambrian: Episodes Journal of International Geoscience, v. 7, p. 12–19.

STEINER, M. AND REITNER, J., 2001, Evidence of organic structures in Ediacara-type fosils and associated microbial mats: Geology, v. 29, p. 1119–1122, doi: 10.1130/0091-7613(2001)029<1119.

TARHAN, L.G., DROSER, M.L., AND GEHLING, J.G., 2015, Depositional and preservational environments of the Ediacara Member, Rawnsley Quartzite (South Australia): Assessment of paleoenvironmental proxies and the timing of "ferruginization": Palaeogeography, Palaeoclimatology, Palaeoecology, v. 434, p. 4–13, doi: 10.1016/j.palaeo.2015.04.026.

TARHAN, L.G., HUGHES, N.C., MYROW, P.M., BHARGAVA, O.N., AHLUWALIA, A.D., AND KUDRYAVTSEV, A.B., 2014, Precambrian-Cambrian boundary interval occurrence and form of the enigmatic tubular body fossil *Shaanxilithes ningqiangensis* from the Lesser Himalaya of India: Palaeontology, v. 57, p. 283–298, doi: 10.1111/pala.12066.

TOWE, K.M., 1970, Oxygen-collagen priority and the early metazoan fossil record, Proceedings of the National Academy of Science, v. 65, p. 781-788.

VINTHER, J., 2015, The origins of molluscs: Palaeontology, v. 58, p. 19–34, doi: 10.1111/pala.12140.

WADE, M., 1968, Preservation of soft-bodied animals in Precambrian sandstones at Ediacara, South Australia: Lethaia, v. 1, p. 238–267, doi: 10.1111/j.1502-3931.1968.tb01740.x.

XIAO, S. AND LAFLAMME, M., 2009, On the eve of animal radiation: phylogeny, ecology and evolution of the Ediacara biota: Trends in Ecology & Evolution, v. 24, p. 31–40, doi:

C

10.1016/j.tree.2008.07.015.

ZHURALEV, A.Y., 1993, Were Ediacaran Vendobionta multicellulars? Neues Jahrbuch fur Geologie und Palaontologie. Abhandlungen1, v. 190, p. 299–314.